Pergamon

Tetrahedron 54 (1998) 1867–1900

TETRAHEDRON

The Quantitation of the Competing Energetics of the Stereoelectronic and Steric Effects of the 3'-OH and the Aglycone in the α- versus β-D- & -L-2'-deoxyribonucleosides by ^{1}H-NMR

Christophe Thibaudeau, András Földesi and Jyoti Chattopadhyaya*

Department of Bioorganic Chemistry, Box 581, Biomedical Centre,
University of Uppsala, S-751 23 Uppsala, Sweden

(E-mail: jyoti@bioorgchem.uu.se. Fax: +4618554495)

Received 26 September 1997; revised 28 November 1997; accepted 4 December 1997

Abstract: By comparative NMR study of 2',3'-dideoxynucleosides (see ref 1) with α-D- or L-2'-deoxynucleosides, we have been able to quantify for the first time the competing medium-dependent influences of the 3'-OH promoted gauche and the aglycone-configuration dependent anomeric effects that result in the overall drive of the sugar conformation in 2'-deoxynucleosides. It has been shown that although the pK_as of the nucleobases in α- and β-D-2-deoxynucleosidess are identical, the transmission of the free-energy of protonation-deprotonation equilibria to steer the sugar conformation is not the same, indeed it is finely tuned by the balance between the 3'-gauche and anomeric effect. It has emerged that the counteracting 3'-OH gauche effect reduces the influence of the pH-dependent anomeric effect, thereby limiting the conformational flexibility of β-D-2'-deoxynucleosides with respect to the corresponding β-D-2',3'-dideoxynucleosides.

The evolutionery choice of chirality has been the molecular basis of life. The β-D-2'-deoxynucleosides (β-D-dNs) are the building blocks of natural DNA, whereas the unnatural β-L-DNA is its mirror image, consisting of β-L-2'-deoxynucleosides (β-L-dNs). The mirror-image relationship of the natural DNA and of the unnatural β-L-DNA is well known and has been unambiguously demonstrated by the identical X-ray crystal structures of D-d(CGCGCG) and of its L counterpart[3]. It has been shown that the oligomerization of activated guanosine mononucleotides in the presence of poly(C) template is easily achieved if both the template and the monomers are of the same handedness, whereas it is much less efficient with the racemic D/L-mixture of the monomer, and that monomers of opposite handedness inhibit the progress of the oligomerization by acting as chain terminators due to their incorporation at the 2'(3') end of the oligomer[4]. The racemization of biomolecules gives reduced biological activity, which has been attributed to the unfavourable changes in the highly-ordered structure.

Only a few nucleosides with α-configuration at the anomeric center have been found in nature[5-7]. The biological activities of α-2'-deoxy-6-thioguanosine (antitumor)[8], α-4'-thio-5-fluorouridine (bacteriostatic)[9], 9-(α-D-arabinofuranosyl)-adenine (cytostatic)[10] and a few C2 derivatives of 2'-deoxyadenosine (inhibitors of the

0040-4020/98/$19.00
PII: S0040-4020(97)10403-3

growth of certain organisms[11]) have been reported. Using simple Dreiding stereomodels, Sequin has been the first one to postulate[12] that a chain of α-nucleotides could form a double helix featuring the same properties as the natural DNA helix, *i.e.* stabilizing intra- or inter-strands interactions through Watson-Crick base-pairing and base-base stacking, both with its complementary α-strand (provided that both chains have an opposite polarity) and with its complementary β-strand (both chains having the same polarity). More recently, Imbach *et. al.* confirmed Sequin's predictions using hyperchromocity and NMR experiments with α-hexadeoxyribonucleotides[13].

To the best of our knowledge, neither an experimental comparison of the intramolecular stereoelectronic energetics of β-D-dNs as building blocks of Nature vis-a-vis their mirror-image β-L-counterparts nor the origin of the choice of β-D-dNs as the molecules for the storage of genetic information over α-D-dNs have been reported hithertofore. In α-D-dNs and β-D-dNs, the competing stereoelectronic influence of the anomeric effect (and its associated counteracting steric effect, *vide infra*) resulting from the C1'-nucleobase and of the 3'-OH induced gauche effect ([O3'-C3'-C4'-O4']) drives the two-state N⇄ S pseudorotational equilibrium. In order to dissect the relative influences of the anomeric effect and the 3'-OH gauche effect upon the inherent flexibility of sugar conformation in the natural 2'-deoxynucleosides (dNs), we first chose simpler 2',3'-dideoxynucleosides (ddNs) as models to investigate the strength of the C1' configuration-dependent pure anomeric effect[1]. This work showed[1] for the first time that the configuration of the C1' aglycone indeed dictates the conformational flexibilities of β-D-ddNs more effectively than in α-D-ddNs. This has enabled us in the present work to delineate the competing influence of the steric and stereoelectronic effects of 3'-OH moiety on the modulation of the strength of the anomeric effect in the naturally ubiquitous 2'-deoxynucleosides in α and β anomers in comparison with their ddN counterparts.

We herein show that (i) The pK_as of the nucleobases in dNs remain unchanged, within the experimental accuracy, as the configuration at C1' is inverted from β- to α-, as in the ddN series, suggesting that the electronic character of the nucleobase is the same in α- and β-nucleosides and that 3'-OH has no effect. (ii) The conformational preferences in β-D-dA and 3',5'-diOMe-β-D-dA are the same, which means that 5'-OH and the C1'-aglycone do not interact in β-dNs through intramolecular hydrogen-bond. (iii) While all β-D-ddNs prefer the N-type pseudorotamers, the sugar moiety in β-D-dNs prefer S-type conformers, showing the opposing influence of the [O3'-C3'-C4'-O4'] gauche effect and of the anomeric effect. (iv) In the whole β-D-ddN and β-D-dN series, the 3'-OH gauche effect, the anomeric effect and the entropy of the system are modulated by the pD of the medium. The overall influence of the opposing 3'-OH gauche effect in β-D-dNs is experimentally evidenced by the weakening of the pD-dependent strength of the anomeric effect by a factor of 2 - 4 compared to β-D-ddN counterparts. (v) α-D-dA, 3'-OMe-α-D-dA, and 3',5'-diOMe-α-D-dA show the same pD-dependent conformational preferences, suggesting that the 3'-OH and the nucleobase are not involved in any intramolecular H-bonding interaction in α-D-dNs. This is supported by the fact that the nucleobase preferentially adopts *anti*-type orientation around the glycosidic torsion in all α-D-dNs at any pD. (vi) As in α-D-ddA, the preference for the S-type pseudorotamers in α-D-dA [and its 3'-OMe and 3',5'-diOMe derivatives] is not modulated by the pD of the solution due to the fact that both the stereoelectronic forces driving its sugar conformation and the -TΔS° term are pD-insensitive. (vii) The strength of the anomeric effect is less efficiently modulated by protonation in α-D-dG than in α-D-ddG, showing the effect of 3'-OH in the former. (viii) The strength of the stereoelectronic forces (ΔH° term) that drive the sugar conformation is much less efficiently modulated by the pD of the solution in pyrimidine α-D-dNs compared to the corresponding β-D-dNs, just as in

pyrimidine α-D- versus β-D-ddNs series[1]. (ix) The actual pD-dependent conformational preference of the sugar moiety in pyrimidine α-D/L-dNs is steered *more efficiently* than in the β-counterparts owing to the entropic reasons (-TΔS° term).

Methodology

The determination of the energetics of the two-state N ⇄ S equilibrium in α- or β-D- and -L-dNs, and their comparison with the results obtained in our previous study on α-D-ddNs versus β-D-ddNs[1] has been performed using our published procedure[21] basing on the pseudorotational analysis and the van't Hoff plots.

(1) Pseudorotational Concept.

The continuous interconversions of puckered forms of pentofuranose moieties in nucleosides are the basis of the pseudorotation concept[14a]. The conformation of each pseudorotamer can be simply described by the phase angle of pseudorotation (P) and by the puckering amplitude (Ψ_m); the former indicates which part of the furanose ring is mostly puckered, whereas the latter reflects the extent of the puckering[14b,c]. The hypothesis of the dynamic two-state N ⇄ S pseudorotational equilibrium in solution (Scheme 1 for ddNs, Scheme 2 for dNs), originally based on the analysis of the statistical distribution of the X-ray crystal structures of nucleosides[15], has been further corroborated by the NMR observations of the two distinctly identifiable and dynamically interconverting N⇄ S conformations as evident by their respective chemical shifts and $^3J_{HH}$ of the constituent sugar moieties in B ⇄ Z DNA[16] or A ⇄ Z RNA[17] or in the A-form ⇄ B-form lariat RNA[18]. Using ^{1}H-NMR spectroscopy, the validity of the two-state N ⇄ S equilibrium of nucleosides in aqueous solution has been further evidenced by us[2] in that the estimation of its pD-dependent energetics (*vide infra*) of N ⇄ S equilibrium for all 2'-deoxy- and ribonucleosides can be used to reproduce the literature values[19] of the pK_a of the constituent nucleobases.

(2) Nomenclature for D- and L-Nucleosides.

In D-nucleosides, the standard N (P = 0°) and S (P = 180°) conformations correspond to those in which the [C1'-C2'-C3'-C4'] torsion angle has a maximal positive and maximal negative value, respectively, whereas it is the opposite in the L-enantiomers because of their mirror-image relationship as defined by Hoffman and Altona[20] (Scheme 2).

(3) Determination of the Thermodynamics of the N ⇄ S Equilibrium in Nucleosides.

We have shown[21] that the temperature and pD-dependent study of the sensitive two-state N ⇄ S equilibrium in D_2O solution allows us to take an experimental energy inventory of the forces that control the sugar conformation in β-D-nucleos(t)ides. We have used this published methodology to assess the conformational preferences of the sugar moieties in α-D-dNs **9**, **17**, **20** and **24**, 3'-OMe-α-D-dA **11**, 3',5'-diOMe-α-D-dA **12** α-L-dNs **10**, **21** and **25**, β-D-dNs **13**, **18**, **22** and **26**, 3'-OMe-β-D-dA **15**, 3',5'-diOMe-β-D-dA **16**, β-L-dNs **14**, **19**, **23** and **27** in D_2O solution as a function of pD (Scheme 2) as well as ddNs[1] **1** - **8** (Scheme 1) and the abasic sugars[1,21a] **28** - **31** (Scheme 3).

The thermodynamics of the N ⇄ S equilibrium of the pentofuranose moiety in dNs **9** - **27** have been calculated[21] from van't Hoff plots based on the temperature variation of the mole fractions of N and S

pseudorotamers at various acidic, neutral and alkaline pDs using the computer program PSEUROT[22] from the vicinal $^3J_{HH}$ coupling constants extracted from 1D ^{1}H-NMR spectra [for $^3J_{HH}$ see Tables 9 for α-D-dA (**9**), **10** for α-D-dG (**17**), 11 for α-D-dC (**20**), 12 for α-D-T (**24**) and 13 for α- and β-L-dNs as well as for **11**, **12**, **15** and **16**]. The enthalpy (ΔH°) and entropy ($-T\Delta S^\circ$) contributions to the free-energy (ΔG°) at 298 K of the N⇄ S equilibrium are presented at each pD in Tables 3 - 6 for α-D-dNs. The geometries of the N-type and S-type pseudorotamers optimized by PSEUROT are given at each pD in Tables 3 and 6 for α-D-dNs or in the Experimental Section for α- or β-L-dNs and for **11**, **12**, **15** and **16**.

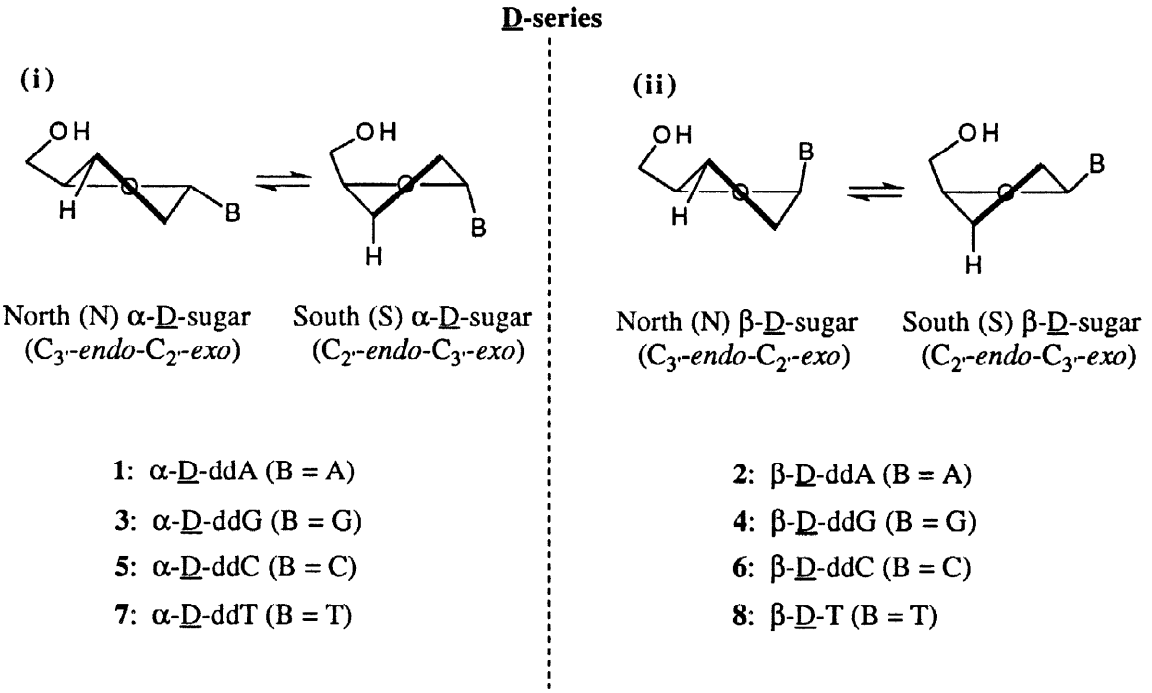

Scheme 1 : The two-state dynamic N⇌S sugar equilibrium in α-D-ddNs **(i)** and β-D-ddNs **(ii)**. The effect of the nucleobase (*i.e.* anomeric + steric) drives the sugar conformation toward N-sugars in β-D-ddNs and toward S-type sugars in α-D-ddNs

The comparative plots of ΔH° and ΔG° as a function of pD are shown in Figure 1 for α-D-ddNs and their β-D-counterparts β-D-ddNs (data taken from ref 1) and in Fig 2 for α-D-dNs and their β-D-counterparts β-D-dNs. The sigmoidal curves shown in Figs 1 and 2 have been fitted to our experimental data, using the Henderson-Hasselbach equation[2], giving the ΔH° and ΔG° values in each of the protonated (P), neutral (N) and deprotonated (D) states of the nucleosides, as well as the pK_as of their nucleobases whenever possible [see Table 1 for ddNs, Table 2 for dNs]. For α-L-dNs, β-L-dNs, 3'-OMe-α-D-dA, 3',5'-diOMe-α-D-dA, 3'-OMe-β-D-dA and 3',5'-diOMe-β-D-dA, ΔH°, ΔS° and ΔG° have been calculated only at one pD at each of the fully protonated, neutral and deprotonated states (See the Experimental Section and Table 2). The data presented in

D-series | **L-series**

(i)

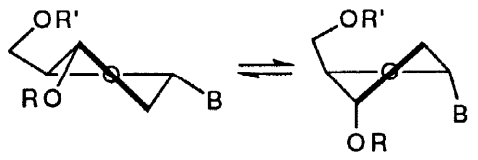

North (N) α-D-sugar ($C_{3'}$-*endo*-$C_{2'}$-*exo*) ⇌ South (S) α-D-sugar ($C_{2'}$-*endo*-$C_{3'}$-*exo*)

9: α-D-dA (B = A, R = R' = H)
11: 3'-OMe-α-D-dA (B = A, R = Me, R' = H)
12: 3',5'-diOMe-α-D-dA (B = A, R = R' = Me)
17: α-D-dG (B = G, R = R' = H)
20: α-D-dC (B = C, R = R' = H)
24: α-D-T (B = T, R = R' = H)

(ii)

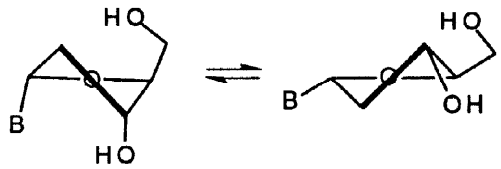

South (S) α-L-sugar ($C_{2'}$-*endo*-$C_{3'}$-*exo*) ⇌ North (N) α-L-sugar ($C_{2'}$-*exo*-$C_{3'}$-*endo*)

10: α-L-dA (B = A)
21: α-L-dC (B = C)
25: α-L-T (B = T)

(iii)

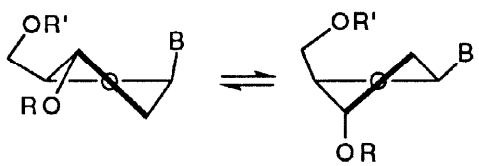

North (N) β-D-sugar ($C_{3'}$-*endo*-$C_{2'}$-*exo*) ⇌ South (S) β-D-sugar ($C_{2'}$-*endo*-$C_{3'}$-*exo*)

13: β-D-dA (B = A, R = R' = H)
15: 3'-OMe-β-D-dA (B = A, R = Me, R' = H)
16: 3',5'-diOMe-β-D-dA (B = A, R = R' = Me)
18: β-D-dG (B = G, R = R' = H)
22: β-D-dC (B = C, R = R' = H)
26: β-D-T (B = T, R = R' = H)

(iv)

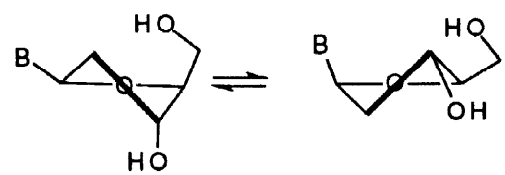

South (S) β-L-sugar ($C_{2'}$-*endo*-$C_{3'}$-*exo*) ⇌ North (N) β-L-sugar ($C_{2'}$-*exo*-$C_{3'}$-*endo*)

14: β-L-dA (B = A)
19: β-L-dG (B = G)
23: β-L-dC (B = C)
27: β-L-T (B = T)

A = adenin-9-yl G = guanin-9-yl C = cytosin-1-yl T = thymin-1-yl

Scheme 2 : The D- and L- mirror image relationship for the two-state dynamic N ⇌ S sugar equilibrium in α-D-dNs **(i)** , α-L-dNs **(ii)**, β-D-dNs **(iii)** and β-L-dNs **(iv)**. In L-nucleosides, the N sugar is redifined as being the form with maximal negative value for the endocyclic torsion [C1'-C2'-C3'-C4'][20]. *Note that in α-D-dNs (i) and α-L-dNs (ii), the aglycone B becomes more pseudoaxial as the anomeric effect becomes stronger in the S-type conformation, whereas in β-D-dNs (iii) and β-L-dNs (iv), this is achieved in the N-type conformation. Hence, the sign for the energetic drive of the anomeric effect in α-nucleosides is opposite to that of β-counterparts.*

Table 1. Thermodynamics of the N ⇄ S pseudorotational equilibria of α-D-ddNs **1**, **3**, **5**, **7** and β-D-ddNs **2**, **4**, **6** and **8** with fully protonated, neutral and fully deprotonated nucleobases[a] and the corresponding pKa values.[b]

Compound	The energetics of N ⇄ S equilibrium when the nucleobase is fully protonated				pK_a [b]	The energetics of N ⇄ S equilibrium when the nucleobase is neutral				pK_a [b]	The energetics of N ⇄ S equilibrium when the nucleobase is fully deprotonated			
	ΔH°_P	ΔS°_P	$-T\Delta S^\circ_P$	ΔG°_P		ΔH°_N	ΔS°_N	$-T\Delta S^\circ_N$	ΔG°_N		ΔH°_D	ΔS°_D	$-T\Delta S^\circ_D$	ΔG°_D
α-D-ddA (1)	-1.7 (0.1)	-0.6 (0.5)	0.2 (0.1)	-1.5 (0.1)	-	-1.7 (0.1)	-0.6 (0.5)	0.2 (0.1)	-1.5 (0.1)	-	-	-	-	-
β-D-ddA (2)	9.2 (0.1)	17.5 (0.1)	-5.0 (0.1)	4.1 (0.1)	3.6	3.5 (0.1)	3.5 (0.4)	-0.9 (0.1)	2.6 (0.1)	-	-	-	-	-
α-D-ddG (3)	-8.7	-20.8	6.0	-2.7	2.7	-0.4 (0.2)	3.1 (0.6)	-0.9 (0.2)	-1.2 (0.1)	-	-0.4 (0.2)	3.1 (0.6)	-0.9 (0.2)	-1.2 (0.1)
β-D-ddG (4)	23.6	59.3	-17.1	6.7	2.5	3.4 (0.4)	1.0 (1.0)	-0.3 (0.2)	2.9 (0.1)	9.5	1.4 (0.1)	-1.7 (0.2)	0.5 (0.1)	1.8 (0.1)
α-D-ddC (5)	-2.9 (0.2)	-4.7 (0.7)	1.4 (0.2)	-1.5 (0.1)	-	-2.9 (0.2)	-4.7 (0.7)	1.4 (0.2)	-1.5 (0.1)	-	-	-	-	-
β-D-ddC (6)	9.6 (0.2)	17.0 (0.4)	-4.9 (0.1)	4.6 (0.1)	4.2	6.6 (0.1)	10.4 (0.2)	-3.0 (0.1)	3.5 (0.1)	-	-	-	-	-
α-D-ddT (7)	-	-	-	-	-	-1.1 (0.1)	-2.0 (0.1)	0.6 (0.1)	-0.5 (0.1)	10.1	-0.5 (0.1)	-1.0 (0.1)	0.3 (0.1)	-0.2 (0.1)
β-D-ddT (8)	-	-	-	-	-	5.4 (0.1)	7.4 (0.1)	-2.2 (0.1)	3.2 (0.1)	9.8	3.5 (0.1)	3.7 (0.3)	-1.1 (0.1)	2.4 (0.1)

[a] These data are taken from ref. 1. ΔH°, $-T\Delta S^\circ$ (at 288 K for **1** - **4**, at 298K for **5** - **8**) and ΔG° are in $kJmol^{-1}$, ΔS° in $Jmol^{-1}K^{-1}$. Their standard deviations (σ) are indicated in parentheses. The 'N', 'P' and 'D' subscripts denote the neutral, the protonated state and the deprotonated states, respectively. The plateaus in the P, N and D states for ΔH°, ΔS° and ΔG° values have been obtained by MonteCarlo fit of the experimental pH-dependent ΔH°, ΔG° (Fig. 1) and ΔS° (not shown) values. [b] Except for α-D-ddG and β-D-ddG in the acidic range, the pK_a values have been calculated through plots of experimental ΔG° of N ⇄ S pseudorotational equilibria as a function of pH and from the Hill plots of pH as a function of $\log(\Delta\Delta G^\circ_{tot} - \Delta\Delta G^\circ / \Delta\Delta G^\circ)$ (not shown). $\Delta\Delta G^\circ_{tot}$ is a total change in ΔG° values between the N and the D/P states, whereas $\Delta\Delta G^\circ$ is the change in ΔG° value at a given pH relative to the reference N state. The pK_a values were also independently determined from Hill plots based on the change in ^{1}H-NMR chemical shifts of aromatic and anomeric protons in **1** - **8** as a function of pH: for α-D-ddA [pK_a = 3.7, 3.7 and 3.6 from δ(H8), δ(H2) and δ(H1'), respectively]; for β-D-ddA [pK_a = 3.7, 3.8 and 3.8 from δ(H8), δ(H2) and δ(H1'), respectively]; for α-D-ddG [pK_a = 2.7 and 2.6 from δ(H8) and δ(H1') in the acidic range and pK_a = 9.7 from δ(H8) in the alkaline range]; for β-D-ddG [pK_a = 2.6 and 2.5 from δ(H8)) and δ(H1') in the acidic range and pK_a = 9.6 from δ(H8)) and δ(H1') in the alkaline range]; for α-D-ddC [pK_a = 4.1 from δ(H6)) and δ(H5)]; for β-D-ddC [pK_a = 4.3 from δ(H6)) and δ(H5)]; for α-D-ddT [pK_a = 9.7, 9.8 and 9.6 from δ(H6)), δ(H1') and δ(C_5-Me)]; for β-D-ddT [pK_a = 9.8, 10.0 and 10.0 from δ(H6)), δ(H1') and δ(C_5-Me)]. In the case of α-D-ddG, β-D-ddG in the acidic pH range, the pK_as calculated from pH-dependent ^{1}H chemical shifts have been used as constraints in the determination of the plateaus in the P and N states for their respective ΔH°, ΔS° and ΔG° values during the MonteCarlo fitting procedure.

Table 2. Thermodynamic data of the dynamic two-state N⇄ S pseudorotational equilibrium in α-D/L-dNs, β-D/L-dNs and abasic sugars with fully protonated, neutral and fully deprotonated nucleobases[a,b] and the corresponding pK_a values.[c]

Compound	The energetics of N ⇄ S equilibrium when the nucleobase is fully protonated [b]			pK_a	The energetics of N ⇄ S equilibrium when the nucleobase is neutral [b]			pK_a	The energetics of N ⇄ S equilibrium when the nucleobase is fully deprotonated [b]		
	ΔH°_P	$-T\Delta S^\circ_P$	ΔG°_P		ΔH°_N	$-T\Delta S^\circ_N$	ΔG°_N		ΔH°_D	$-T\Delta S^\circ_D$	ΔG°_D
α-D-dA (**9**)	-5.0 (0.4)	2.1 (0.3)	-2.8 (0.1)	-	-5.0 (0.4)	2.1 (0.3)	-2.8 (0.1)	-	-	-	-
α-L-dA (**10**)	-5.5 (0.9)	2.7 (0.9)	-2.8 (0.3)	-	-6.0 (0.5)	3.2 (0.6)	-2.9 (0.4)	-	-	-	-
3'-OMe-α-D-dA (**11**)	-5.8 (1.5)	0.8 (1.5)	-4.9 (0.3)	-	-6.4 (0.8)	1.9 (0.7)	-4.5 (0.3)	-	-	-	-
3',5'-diOMe-α-D-dA (**12**)	-5.3 (1.3)	0.8 (1.2)	-4.7 (0.3)	-	-5.8 (0.8)	1.6 (0.7)	-4.1 (0.3)	-	-	-	-
β-D-dA (**13**)	-0.7 (0.1)	-0.4 (0.1)	-1.1 (0.1)	3.5	-3.9 (0.2)	1.8 (0.1)	-2.1 (0.1)	-	-	-	-
β-L-dA (**14**)	-1.2 (0.6)	0.1 (0.6)	-1.1 (0.1)	-	-3.9 (0.3)	1.8 (0.4)	-2.2 (0.2)	-	-	-	-
3'-OMe-β-D-dA (**15**)	-1.4 (0.6)	-0.7 (0.6)	-2.2 (0.2)	-	-4.6 (0.4)	1.4 (0.4)	-3.2 (0.2)	-	-	-	-
3',5'-diOMe-β-D-dA (**16**)	-1.0 (0.6)	-0.7 (0.6)	-1.7 (0.2)	-	-3.6 (0.4)	1.5 (0.4)	-2.1 (0.2)	-	-	-	-
α-D-dG (**17**)	-10.7 (2.0)	6.4 (2.0)	-4.4 (0.3)	2.6	-4.5 (0.5)	2.7 (0.5)	-1.9 (0.1)	-	-3.4 (0.5)	1.4 (0.5)	-1.9 (0.1)
β-D-dG (**18**)	2.1 (0.1)	-2.2 (0.2)	-0.1 (0.1)	2.3	-2.8 (0.2)	1.1 (0.2)	-1.7 (0.1)	9.5	-4.9 (0.2)	2.2 (0.2)	-2.7 (0.1)
β-L-dG (**19**)	1.3 (0.8)	-1.6 (0.8)	-0.3 (0.1)	-	-2.7 (0.3)	0.9 (0.4)	-1.8 (0.2)		-4.3 (0.4)	1.7 (0.4)	-2.6 (0.2)
α-D-dC (**20**)	-7.1 (0.3)	2.5 (0.8)	-4.3 (0.2)	4.1	-7.1 (0.3)	4.0 (0.5)	-3.1 (0.2)	-	-	-	-
α-L-dC (**21**)	-7.3 (0.6)	3.0 (0.6)	-4.2 (0.2)	-	-7.2 (0.5)	4.1 (0.6)	-3.1 (0.2)				
β-D-dC (**22**)	0.0 (0.1)	-0.8 (0.1)	-0.8 (0.1)	4.2	-0.7 (0.1)	-0.5 (0.1)	-1.3 (0.1)	-	-	-	-
β-L-dC (**23**)	-0.2 (0.3)	-0.6 (0.3)	-0.8 (0.1)	-	-0.7 (0.3)	-0.5 (0.3)	-1.2 (0.1)	-	-	-	-
α-D-T (**24**)	-	-	-	-	-4.0 (0.2)	2.0 (0.5)	-2.1 (0.2)	9.8	-4.0 (0.2)	2.7 (0.4)	-1.1 (0.1)
α-L-T (**25**)	-	-	-	-	-4.2 (0.4)	2.1 (0.5)	-2.1 (0.2)	-	-3.4 (0.2)	2.5 (0.4)	-1.0 (0.1)
β-D-T (**26**)	-	-	-	-	-1.4 (0.2)	0.1 (0.1)	-1.3 (0.1)	9.7	-1.9 (0.2)	0.3 (0.2)	-1.6 (0.1)
β-L-T (**27**)	-	-	-	-	-1.2 (1.1)	0.0 (1.0)	-1.2 (1.5)	-	-2.3 (0.7)	0.6 (0.6)	-1.7 (0.9)
THFA (**28**)	-	-	-	-	0.4 (0.3)	-0.3 (0.3)	0.1 (0.4)	-	-	-	-
THFA-OH (**29**)	-	-	-	-	-4.1 (0.3)	1.5 (0.3)	-2.6 (0.4)	-	-	-	-
3'-OMe-THFA (**30**)	-	-	-	-	-4.6 (0.4)	1.2 (0.3)	-3.4 (0.5)	-	-	-	-
3',5'-diOMe-THFA (**31**)	-	-	-	-	-4.2 (0.4)	0.9 (0.3)	-3.3 (0.5)	-	-	-	-

[a] ΔH°, $-T\Delta S^\circ$ (at 298 K) and ΔG° (at 298 K) are in kJmol^{-1}. Their standard deviations (σ) are indicated in parentheses. The 'N', 'P' and 'D' subscripts denote the neutral, the protonated state and the deprotonated states, respectively. ΔH°, $-T\Delta S^\circ$ and ΔG° are taken from ref. 2 for β-D-dNs, from ref. 1 for **30** and **31**, from ref. 21a for **28** and **29**. [b] For α-D-dA, ΔH°, $-T\Delta S^\circ$ and ΔG° in the P and N states have been assumed identical and calculated by averaging the individual corresponding values from pD 1.6 to pD 6.5 (see Tables 2 and 3 and Fig 2), as they are nearly pD-independent. For α-D-dG, the plateaus in the P, N and D states for ΔH°, ΔS° and ΔG° values have been obtained by MonteCarlo fit of the experimental pD-dependent ΔH°, ΔG° and ΔS° values (see Tables 2 and 4 and Fig

2). ΔH° in the P and N states of α-D-dC have been assumed identical and calculated by averaging the individual data from pD 2.0 to pD 7.1 as ΔH° values are nearly pD-independent, whereas the plateaus in the P and N states for $-T\Delta S^{\circ}$ and ΔG° values have been obtained by MonteCarlo fit of the experimental pD-dependent $-T\Delta S^{\circ}$ and ΔG° values (see Tables 2 and 5 and Fig 2). ΔH° in the N and D states of α-D-T have been assumed identical and calculated by averaging the individual data from pD 6.0 to pD 11.6 as ΔH° values are nearly pD-independent, whereas the plateaus in the N and D states for $-T\Delta S^{\circ}$ and ΔG° values have been obtained by MonteCarlo fit of the experimental pD-dependent $-T\Delta S^{\circ}$ and ΔG° values (Tables 2 and 6 and Fig 2). For all α/β-L-dNs, and for compounds **11**, **12**, **15** and **16**, ^{1}H-NMR spectra have been recorded only at two (or three) pDs at which their nucleobases are in the neutral and fully protonated (and/or deprotonated) forms (see experimental section for details). [c] The pK_a values of the constituent nucleobases reported here have been calculated through plots of experimental ΔG° of N⇄S pseudorotational equilibria as a function of pH and from the Hill plots of pH as a function of $\log(\Delta\Delta G^{\circ}_{tot} - \Delta\Delta G^{\circ}/\Delta\Delta G^{\circ})$ (not shown). $\Delta\Delta G^{\circ}_{tot}$ is a total change in ΔG° values between the N and the D/P states, whereas $\Delta\Delta G^{\circ}$ is the change in ΔG° value at a given pH relative to the reference N state. The pK_a values were also independently determined from Hill plots based on the change in ^{1}H-NMR chemical shifts of aromatic and anomeric protons in α-D-dNs as a function of pH: For α-D-dA [pK_a = 3.6, 3.5 and 3.6 from δ(H8) (Panel (A) in Fig 3), δ(H2) and δ(H1'), respectively]; For 3',5'-diOMe-α-D-dA [pK_a = 3.8 and 3.7 from δ(H8) (Panel (B) in Fig 3) and δ(H1'), respectively]; For 3',5'-diOMe-β-D-dA [pK_a = 3.5 from δ(H8) (Panel (F) in Fig 3) and δ(H1'); For α-D-dG [pK_a = 2.6 and 2.4 from δ(H8) (Panel (C) in Fig 3) and δ(H1'), respectively in the acidic range and pK_a = 9.5 from δ(H8) (Panel (C) in Fig 3) in the alkaline range]; For α-D-dC [pK_a = 4.1 and 4.2 from δ(H6) (Panel (D) in Fig 3) and δ(H5), respectively]; For α-D-T [pK_a = 9.9 and 9.7 from δ(H6) (Panel (E) in Fig 3) and δ(C_5-Me), respectively].

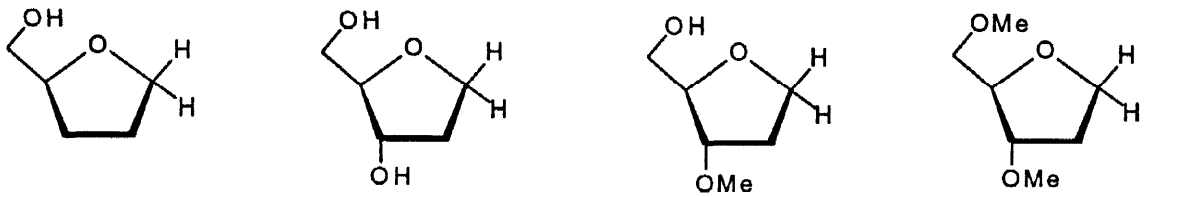

28 (THFA) **29** (THFA-OH) **30** (3'-OMe-THFA) **31** (3,5'-diOMeTHFA)

Scheme 3 : The abasic sugars **28 - 31**

Table 1 have been taken from ref. 21a for **28** and **29**. ΔH°, ΔS° and ΔG° values in the protonated, neutral anddeprotonated states for **1 - 31** are all shown here as P, N and D subscripts throughout the paper. Note that the positive or negative ΔH°, ΔS° and ΔG° values refer to the drive of the N⇄S equilibrium toward N- or S-type pseudorotamers, respectively.

Results and Discussion

(1) The gauche effect of [O3'-C3'-C4'-O4'] fragment opposes the anomeric effect in β-D-dNs whereas both effects act cooperatively to drive the sugar conformation in α-D-dNs.

Our pD-dependent thermodynamic analysis of the N⇄S equilibrium of interrelated analogs including 1,2,3-trideoxy-, 1,2-dideoxy- and 1-deoxypentofuranose, β-D-ddNs, β-D-dNs, β-D-ribonucleosides and their 3'-phosphomonoesters and diesters has uniquely shown[21] that the conformation of the sugar moiety in β-D-nucleosides is energetically controlled by various stereoelectronic gauche and anomeric effects: (a) the

Table 3. Pseudorotational analyses of temperature-dependent $^3J_{HH}$ (from 278 to 358 K)[a] at twelve different pDs (1.6-6.5), and determination of pD-dependent thermodynamics of the two-state N ⇄ S equilibrium for α-D-dA (**9**).

	Total number of PSEUROT analysis [e]	Ψ_m constrained analyses in PSEUROT [b, c]		P_N and Ψ_m(N) constrained analyses in PSEUROT [c, d]		Slopes and intercepts of various van't Hoff plots from $\ln(x_S/x_N)$ vs 1000/T [f]		Thermodynamics of N ⇄ S equilibrium from van't Hoff plots [f, g]			Thermodynamics of N ⇄ S equilibrium from the average populations [h]
pD		P_N	P_S	P_S	Ψ_m(S)	average slopes (σ)	average intercepts (σ)	ΔH° (σ)	-TΔS° (σ)	ΔG^{298}= ΔH°-TΔS°	ΔG^{298} = -0.298*R$\ln_{av}$ ($x_S/(x_N)$)
1.6	16325	0° - 32°	148° - 167°	142° - 170°	25° - 32°	0.55 (0.10)	-0.71 (0.35)	-4.6 (0.8)	1.8 (0.9)	-2.8 (1.2)	-2.8 (0.3)
2.1	17608	0° - 35°	145° - 172°	139° - 171°	25° - 33°	0.66 (0.11)	-1.09 (0.39)	-5.5 (0.9)	2.7 (1.0)	-2.8 (1.3)	-2.8 (0.3)
2.5	15049	4° - 31°	146° - 163°	143° - 168°	25° - 32°	0.66 (0.07)	-1.05 (0.26)	-5.5 (0.6)	2.6 (0.7)	-2.9 (0.9)	-2.9 (0.3)
2.8	16150	0° - 25°	146° - 162°	138° - 170°	24° - 32°	0.60 (0.07)	-0.85 (0.26)	-5.0 (0.6)	2.1 (0.6)	-2.9 (0.9)	-2.9 (0.3)
3.2	15156	0° - 28°	147° - 167°	140° - 173°	24° - 31°	0.56 (0.07)	-0.72 (0.26)	-4.6 (0.6)	1.8 (0.6)	-2.9 (0.9)	-2.9 (0.3)
3.7	14189	0° - 24°	148° - 169°	139° - 176°	22° - 29°	0.53 (0.06)	-0.66 (0.24)	-4.4 (0.5)	1.6 (0.6)	-2.8 (0.8)	-2.8 (0.3)
4.0	14697	0° - 23°	147° - 169°	139° - 178°	22° - 28°	0.60 (0.06)	-0.87 (0.24)	-5.0 (0.5)	2.2 (0.6)	-2.9 (0.8)	-2.9 (0.4)
4.2	12520	0° - 33°	146° - 193°	140° - 181°	21° - 28°	0.57 (0.06)	-0.78 (0.24)	-4.7 (0.5)	1.9 (0.6)	-2.8 (0.8)	-2.9 (0.3)
4.6	14787	0° - 35°	147° - 197°	140° - 182°	20° - 28°	0.64 (0.06)	-1.00 (0.24)	-5.3 (0.5)	2.5 (0.6)	-2.9 (0.8)	-2.9 (0.4)
5.0	14164	0° - 36°	149° - 196°	140° - 182°	20° - 28°	0.61 (0.06)	-0.92 (0.24)	-5.1 (0.5)	2.3 (0.6)	-2.8 (0.8)	-2.8 (0.4)
5.9	14046	0° - 36°	148° - 196°	140° - 182°	20° - 28°	0.57 (0.06)	-0.78 (0.24)	-4.7 (0.5)	1.9 (0.6)	-2.8 (0.8)	-2.8 (0.4)
6.5	13958	0° - 36°	146° - 193°	140° - 183°	20° - 27°	0.63 (0.06)	-0.95 (0.24)	-5.2 (0.5)	2.4 (0.6)	-2.8 (0.8)	-2.8 (0.4)

[a] $^3J_{HH}$ at each of twelve pDs at two extreme temperatures are given in Table 9. [b] At each pD, assuming Ψ_m (N) = Ψ_m (S), we have kept Ψ_m (N) and Ψ_m (S) fixed to identical values in the range from 24° to 33° and surveyed the conformational hyperspace in 1° steps. [c] The error estimates of the PSEUROT analyses have been assessed in terms of ΔJ_{max} and r.m.s. The number of successful PSEUROT analyses in column 2 are designated to those which were within the constrained values (see experimental section) as well as having a ΔJ_{max} and r.m.s. values smaller than 0.6 Hz and 0.3 Hz. [d] P_N of the minor N-type conformers were fixed at -30° ≤ P_N ≤ 30° in 20° steps with Ψ_m (N) being simultaneously fixed at 24°, 28° and 32° at each pD during several PSEUROT optimizations. [e] For each of these PSEUROT[22] calculations the coupling constants were 1000 times randomized (see experimental section). [f] The populations of N and S pseudorotamers obtained through each of the above PSEUROT calculations at different temperatures, shown in column 2, are the basis for the identical number of van't Hoff plots, which in turn were used to calculate the average slope and intercept. [g] The average of the slopes and the intercepts derived from all van' t Hoff plots at a particular pD given in the columns 7 and 8 were finally used to calculate the average ΔH°, -TΔS° (at 298 K) and subsequently ΔG^{298} (kJ/mol^{-1}) of N ⇄ S equilibria of **9**. [h] ΔG^{298} calculated directly from the average logarithm $\ln_{av}$ (x_S/ (1- x_S)), by using the Gibbs equation ΔG^T= -(RT/1000)$\ln_{av}$ (x_S/ (1- x_S)) with 1- x_S =x_N , R is the gas constant and T is the temperature. The standard deviations are in parentheses.

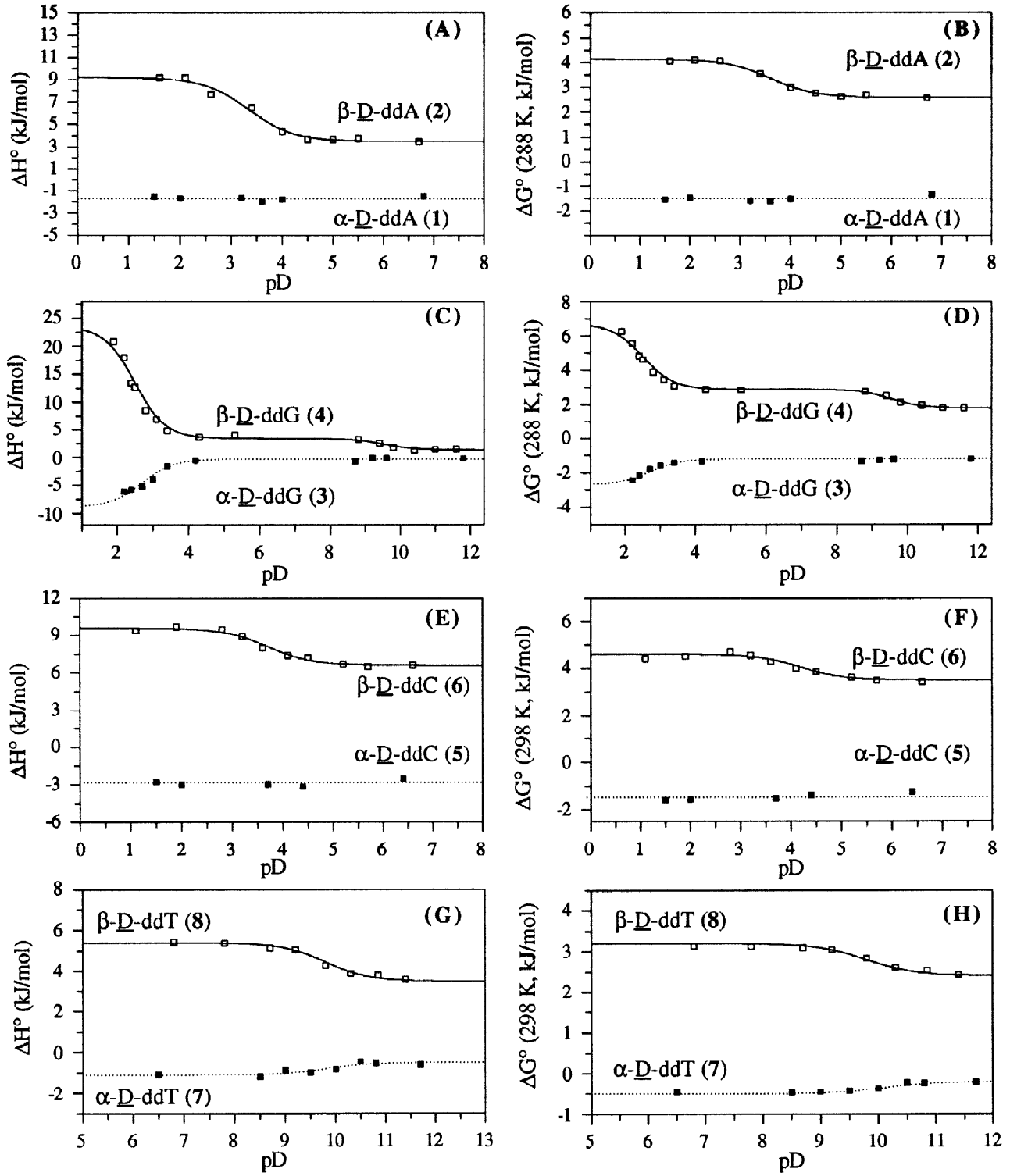

Fig 1 : The plots of experimental ΔH°[Panels (A), (C), (E) and (G)] and ΔG° values [Panels (B), (D), (F) and (H)] for the N ⇄ S pseudorotational equilibrium of α-D-ddNs **1**, **3**, **5** and **7** and β-D-ddNs **2**, **4**, **6** and **8**. The sigmoidal curves have been fitted to our experimental data using a MonteCarlo procedure (see the legend of Table 1, the text and ref. 1 for details). **(A)** ΔH° values (at 6 pDs in the range 1.5 - 6.8) are pD-independent for α-D-ddA (**1**) whereas they show a sigmoidal dependence on pD for its β-counterpart β-D-ddA (**2**) (at 9 pDs in the range 1.6 to 6.7). **(B)** ΔG^{288} values (at 6 pDs in the range 1.5 - 6.8) are pD-independent for

α-D-ddA (1) whereas they show a sigmoidal dependence on pD for its β-counterpart β-D-ddA (2) (at 9 pDs in the range 1.6 to 6.7). **(C)** ΔH° values both for α-D-ddG (3) (at 10 pDs in the range 2.2 - 11.8) and for its β-counterpart β-D-ddG (4) (at 15 pDs in the range 1.9 to 11.6) show a sigmoidal dependence on pD. **(D)** ΔG^{288} values both for α-D-ddG (3) (at 10 pDs in the range 2.2 - 11.8) and for its β-counterpart β-D-ddG (4) (at 15 pDs in the range 1.9 to 11.6) show a sigmoidal dependence on pD. **(E)** ΔH° values for α-D-ddC (5) (at 5 pDs in the range 1.5 - 6.4) are pD-independent, whereas they show a sigmoidal dependence on pD for its β-counterpart β-D-ddC (6) (at 10 pDs in the range 1.1 - 6.6). **(F)** ΔG^{298} values for α-D-ddC (5) (at 5 pDs in the range 1.5 - 6.4) are pD-independent, whereas they are pD-dependent for its β-counterpart β-D-ddC (6) (at 10 pDs in the range 1.1 - 6.6). **(G)** ΔH° values both for for α-D-ddT (7) (at 8 pDs in the range 6.5 - 11.7) and for its β-counterpart β-D-ddT (8) (at 8 pDs in the range 6.8 - 11.4) are pD-dependent. **(H)** ΔG^{298} values both for α-D-ddT (7) (at 8 pDs in the range 6.5 - 11.7) and for its β-counterpart β-D-ddT (8) (at 8 pDs in the range 6.8 - 11.4) are pD-dependent.

anomeric effect[21,23-25] of the nucleobase drives the N⇄ S equilibrium toward N-type conformations giving a pseudoaxial orientation of the aglycone, which is opposed by its counteracting steric bulk favouring its pseudoequatorial orientation. (b) The gauche effects[21,26] of [O3'-C3'-C4'-O4'] and [O2'-C2'-C1'-N(base)] fragments counteract the anomeric effect by pushing the N ⇄ S equilibrium toward S-type pseudorotamers. (c) The gauche effect of [O2'-C2'-C1'-O4'] fragment drives the N⇄ S equilibrium toward N-type conformations, whereas (d) the gauche effect of [O5'-C5'-C4'-O4'] fragment is minimal either in pseudoequatorial (in N-type) or in pseudoaxial orientation (in S-type sugar conformations).

The strengths of these stereoelectronic effects in nucleos(t)ides can be estimated by pairwise comparison of thermodynamics of the N⇄ S equilibrium[21] in nucleosides that differ only by one substituent or by an inversion of the configuration at one particular center. These pairwise comparisons give us an enormous scope to predict and engineer a certain conformational preference in nucleosides and nucleotides simply by changing the nature of the substituent at C1', C2' and C3' and their configuration in the constituent sugar unit[21], in general. At any pD, the conformation of the sugar moiety in all dNs and ddNs is mainly driven by ΔH° contribution to ΔG° of the N⇄ S pseudorotational equilibrium, which clearly prevails over the weaker $-T\Delta S^{\circ}$ term (see Tables 1 and 2 for the thermodynamics of the N⇄ S equilibrium in ddNs and dNs, respectively, in the P, N and D states, Tables 3 - 6 for the ΔH° values at each pD for dNs and ref. 1 for ddNs).

In β-D-ddNs **2**, **4**, **6** and **8** and α-D-ddNs **1**, **3**, **5** and **7**, the effect of the nucleobase (*i.e.* anomeric effect) is solely responsible[1] for the preference of the sugar moiety for N- and S-type pseudorotamers, respectively. In dNs, the gauche effect of [O3'-C3'-C4'-O4'] fragment counteracts and overrides the effect of the nucleobase in the β-series, which results in the preferential S-type puckering of the constituent sugar moiety, as experimentally evidenced by the negative ΔH° values for the N ⇄ S equilibrium in **13**, **18**, **22** and **26** (Table 2).

On the other hand, in α-D-dNs, both the effect of the nucleobase and the effect of [O3'-C3'-C4'-O4'] fragment cooperate to drive the pentofuranose conformation toward S-type sugars, which is reflected in the negative ΔH° values determined for **9**, **17**, **20** and **24** (Table 2).

As expected, owing to the cooperative (or opposing) anomeric and 3'-gauche effects in α-D/L-dNs (β-D/L-dNs), ΔH° term is much more efficient to drive the sugar moiety in α-D- and α-L-dNs toward S-type conformations than for their β counterparts (see Table 2). Larger ΔH° values for α-D/L-dNs than for their β-counterparts also signify that the flexibility of the conformation of the sugar moiety is larger in α-D- and α-L-dNs than in the β counterparts from 278 to 358K, except in the neutral and deprotonated α-D-dG (**17**).

Table 4. Pseudorotational analyses of temperature-dependent $^3J_{HH}$ (from 278 to 358 K)[a] at fourteen pDs (1.0 - 11.6) and determination of the pD-dependent thermodynamics of the two-state N ⇄ S equilibrium in α-D-dG (**17**).

	Total number of PSEUROT analysis [e]	Ψ_m constrained analyses in PSEUROT [b, c]		P_N and Ψ_m(N) constrained analyses in PSEUROT [c, d]		Slopes and intercepts of various van't Hoff plots from $\ln(x_S/x_N)$ vs 1000/T [f]		Thermodynamics of N ⇄ S equilibrium from van't Hoff plots [f, g]			Thermodynamics of N ⇄ S equilibrium from the average populations [h]
pD		P_N	P_S	P_S	Ψ_m(S)	average slopes (σ)	average intercepts (σ)	ΔH° (σ)	-TΔS° (σ)	ΔG^{298}= ΔH°-TΔS°	ΔG^{298} = -0.298*R$\ln_{av}$ ($x_S/(x_N)$)
1.0	13876	5° - 40°	158° - 170°	152° - 169°	30° - 35°	1.31 (0.28)	-2.69 (0.95)	-10.9 (2.3)	6.7 (2.4)	-4.2 (3.3)	-4.3 (0.3)
1.5	15745	2° - 40°	156° - 169°	150° - 168°	30° - 35°	1.23 (0.22)	-2.42 (0.73)	-10.2 (1.8)	6.0 (1.8)	-4.2 (2.6)	-4.2 (0.3)
2.0	15603	1° - 40°	157° - 171°	151° - 170°	29° - 34°	1.09 (0.22)	-1.99 (0.77)	-9.1 (1.9)	4.9 (1.9)	-4.2 (2.7)	-4.2 (0.3)
2.4	13105	-2° - 27°	154° - 168°	147° - 170°	27° - 32°	0.98 (0.11)	-1.85 (0.37)	-8.2 (0.9)	4.6 (0.9)	-3.6 (1.3)	-3.5 (0.3)
2.9	12264	-1° - 24°	147° - 171°	139° - 174°	23° - 31°	0.87 (0.10)	-1.83 (0.35)	-7.2 (0.8)	4.5 (0.9)	-2.7 (1.2)	-2.7 (0.3)
3.5	6082	-7° - 31°	142° - 196°			0.65 (0.06)	-1.32 (0.22)	-5.4 (0.5)	3.3 (0.5)	-2.2 (0.8)	-2.2 (0.1)
4.5	5451	-5° - 27°	145° - 195°			0.62 (0.06)	-1.25 (0.22)	-5.1 (0.5)	3.1 (0.5)	-2.0 (0.8)	-2.0 (0.1)
6.3	6646	-3° - 27°	148° - 196°			0.51 (0.06)	-0.94 (0.20)	-4.2 (0.5)	2.3 (0.5)	-1.9 (0.7)	-1.9 (0.1)
7.3	6634	-2° - 29°	149° - 197°			0.48 (0.06)	-0.85 (0.20)	-4.0 (0.5)	2.1 (0.5)	-1.9 (0.7)	-2.0 (0.1)
8.6	7839	-1° - 30°	158° - 200°			0.48 (0.06)	-0.84 (0.20)	-4.0 (0.5)	2.1 (0.5)	-1.9 (0.7)	-1.9 (0.1)
9.2	7256	2° - 32°	163° - 200°			0.46 (0.06)	-0.79 (0.19)	-3.8 (0.5)	2.0 (0.5)	-1.9 (0.7)	-1.9 (0.1)
10.0	6122	1° - 32°	168° - 200°			0.43 (0.06)	-0.60 (0.20)	-3.5 (0.5)	1.5 (0.5)	-2.1 (0.7)	-2.1 (0.1)
10.6	4939	5° - 35°	169° - 200°			0.43 (0.06)	-0.64 (0.19)	-3.6 (0.5)	1.6 (0.5)	-2.0 (0.7)	-1.9 (0.1)
11.6	3662	4° - 34°	171° - 200°			0.37 (0.06)	-0.44 (0.20)	-3.1 (0.5)	1.1 (0.5)	-2.0 (0.7)	-2.0 (0.1)

[a] $^3J_{HH}$ at each of the fourteen pDs at two extreme temperatures are given inTable 10. [b] Assuming $\Psi_m(N) = \Psi_m(S)$, we have kept $\Psi_m(N)$ and $\Psi_m(S)$ fixed to identical values in the range from 28° to 38° at pD 1.0, 28° to 36° at pD 1.5, 27° to 36° at pD 2.0, 25° to 35° at pD 2.4, 22° to 31° at pD 2.9, 20° to 29° at 3.5 ≤ pD ≤ 7.3, 20° to 28° at pD 8.6 and 9.2, 20° to 27° at pD 10.0, 20° to 26° at pD 10.6 and 11.6 and surveyed the conformational hyperspace in 1° steps during several PSEUROT. [c] The error estimates of the PSEUROT analyses have been assessed in terms of ΔJ_{max} and r.m.s. The number of successful PSEUROT analyses in column 2 are designated to those which were within the constrained values (see experimental section) as well as having a ΔJ_{max} and r.m.s. values smaller than 0.6 Hz and 0.3 Hz. [d] P_N of the minor N-type conformers were fixed at -30° ≤ P_N ≤ 30° in 20° steps with Ψ_m (N) being simultaneously fixed at 30°, 33° and 36° at pD 1.0, 1.5, 2.0, at 27°, 31° and 35° at pD 2.4 and at 22°, 25° and 29° at pD 2.9 during several PSEUROT optimizations which resulted in different populations of N and S conformers with their distinctive P_S and Ψ_m (S). [e] For each of these PSEUROT[22] calculations the coupling constants were 1000 times randomized (see experimental section). [f] The populations of N and S pseudorotamers obtained through each of the above PSEUROT calculations at different temperatures, shown in column 2, are the basis for the identical number of van't Hoff plots, which in turn were used to calculate the average slope and intercept. [g] The average of the slopes and the intercepts derived from all van' t Hoff plots at a particular pD given in the columns 7 and 8 were finally used to calculate the average ΔH°, -TΔS° (at 298 K) and subsequently ΔG^{298} (kJ/mol^{-1}) of N ⇄ S equilibria of **17**. [h] ΔG^{298} calculated directly from the average logarithm $\ln_{av}$ (x_S/ (1- x_S)), by using the Gibbs equation ΔG^T = -(RT/1000)$\ln_{av}$ (x_S/ (1- x_S)) with 1- x_S =x_N , R is the gas constant and T is the temperature. The standard deviations are in parentheses.

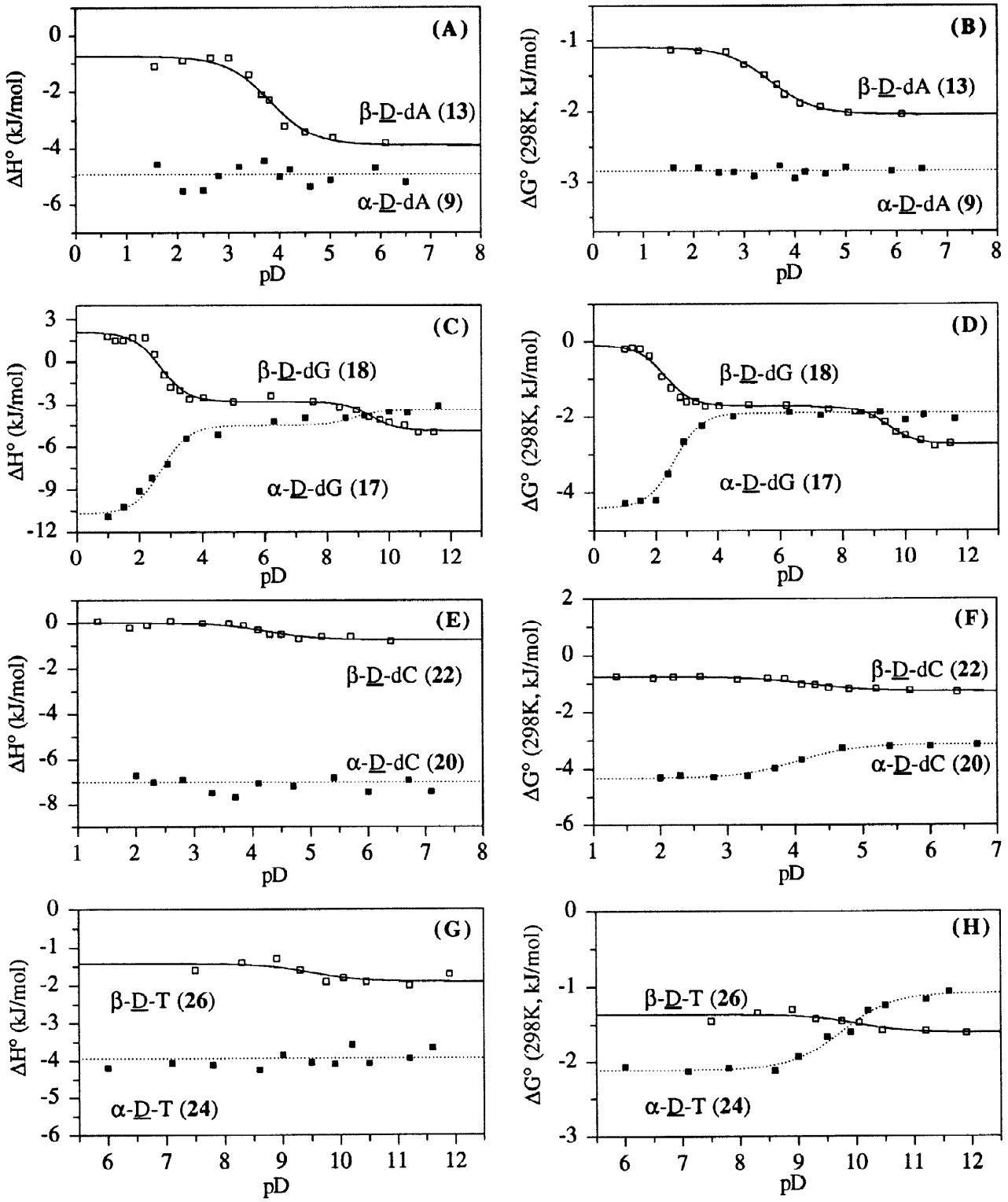

Fig 2 : The plots of experimental ΔH° [Panels (A), (C), (E) and (G)] and ΔG° values [Panels (B), (D), (F) and (H)] for the N ⇄ S pseudorotational equilibrium of α-D-dNs **9**, **17**, **20** and **24** and β-D-dNs **13**, **18**, **22** and **26**. The sigmoidal curves have been fitted to our experimental data using a MonteCarlo procedure (see the legend of Table 2 and the text). **(A)** ΔH° values (at 12 pDs in the range 1.6 - 6.5, Table 9) are pD-independent for α-D-dA (**9**) whereas they show a sigmoidal dependence on pD for its β-counterpart β-D-dA (**13**) (at 11 pDs in the range 1.5 to 6.1, see ref. 2). **(B)** ΔG^{298} values (at 12 pDs in the range 1.6 - 6.5, Table 9) are pD-

independent for α-D-dA (9) whereas they show a sigmoidal dependence on pD for its β-counterpart β-D-dA (13) (at 11 pDs in the range 1.5 to 6.1, see ref. 2). **(C)** ΔH° values both for α-D-dG (17) (at 14 pDs in the range 1.0 - 11.6, Table 10) and for its β-counterpart β-D-dG (18) (at 22 pDs in the range 1.0 to 11.4, see ref. 2) show a sigmoidal dependence on pD. **(D)** ΔG^{298} values both for α-D-dG (17) (at 14 pDs in the range 1.0 - 11.6, Table 10) and for its β-counterpart β-D-dG (18) (at 22 pDs in the range 1.0 to 11.4, see ref. 2) show a sigmoidal dependence on pD. **(E)** ΔH° values for α-D-dC (20) (at 11 pDs in the range 2.0 - 7.0, Table 11) are pD-independent, whereas they show a sigmoidal dependence on pD for its β-counterpart β-D-dC (22) (at 14 pDs in the range 1.3 - 6.4, see ref. 2). **(F)** ΔG^{298} values both for α-D-dC (20) (at 11 pDs in the range 2.0 - 7.0, Table 11) and for its β-counterpart β-D-dC (22) (at 14 pDs in the range 1.3 - 6.4, see ref. 2) show a sigmoidal dependence on pD. **(G)** ΔH° values for α-D-T (24) (at 11 pDs in the range 6.0 - 11.6, Table 12) are pD-independent, whereas they show a sigmoidal dependence on pD for its β-counterpart β-D-T (26) (at 9 pDs in the range 7.5 - 11.9, see ref. 2). **(H)** ΔG^{298} values both for α-D-T (24) (at 11 pDs in the range 6.0 - 11.6, Table 12) and for its β-counterpart β-D-T (26) (at 9 pDs in the range 7.5 - 11.9, see ref. 2) show a sigmoidal dependence on pD.

(2) The pD-dependent modulation of the anomeric effect is more reduced in β-D-dNs than β-D-ddNs as a result of the competing stereoelectronic gauche effect of 3'-OH in the former.

(A) The 5'-OH and the nucleobase do not interact to drive the sugar conformation in β-D-dNs.

Table 2 shows that the pD-dependent conformation of the sugar moiety is nearly the same in β-D-dA (**13**) and 3',5'-diOMe-β-D-dA (**16**), which rules out any hydrogen-bonding interaction between 5'-OH and the C1'-aglycone in β-D-dNs.

In order to investigate the conformation of the constituent nucleobases around the glycosidic torsion in dNs, we have performed a series of 1D ^{1}H nOe difference experiments in which either the aromatic proton of the nucleobase or the anomeric proton have been preirradiated for all α/β-D-dN pairs at one pD in each of their protonated, neutral and/or deprotonated states. Using the method developed by Rosemeyer *et al*[27], the nOe enhancements experimentally obtained have been further translated into the relative populations of *syn* versus *anti* rotamers around the glycosidic torsion (Table 7). Our nOe difference experiments clearly show the predominant *anti*-type orientation of the nucleobase around the glycosidic torsion for all β-D-dNs, preventing any interaction between N3 and 5'-OH proton in purines, between O2 and 5'-OH in pyrimidines.

(B) The gauche effect of 3'-OH in β-D-dNs restricts the conformational flexibility of the sugar in comparison with the β-D-ddNs counterparts.

A perusal of the thermodynamics of the two-state N⇄ S pseudorotational equilibrium in acidic, neutral and alkaline pDs for β-D-ddNs [Table 1 for **2**, **4**, **6** and **8**; Fig 1 for the sigmoidal profiles of the thermodynamic quantities] and β-D-dNs [Table 2 for **13**, **18**, **22** and **26**; Fig 2 for the sigmoidal plots as a function of pD] shows that the modulation of ΔH° contribution to the free-energy ΔG° of the equilibrium is much reduced upon protonation and / or deprotonation of the nucleobase in the dN series than in the ddN series [For dNs: $\Delta\Delta H^{\circ}_{(P-N)}$ = 3.2 kJmol^{-1} for β-D-dA, 3.2 kJmol^{-1} for 3'-OMe-β-D-dA, 2.6 kJmol^{-1} for 3',5'-diOMe-β-D-dA, 4.9 kJmol^{-1} for β-D-dG and 0.7 kJmol^{-1} for β-D-dC; $\Delta\Delta H^{\circ}_{(D-N)}$ = -2.1 kJmol^{-1} for β-D-dG and -0.5 kJmol^{-1} for β-D-T; For ddNs: $\Delta\Delta H^{\circ}_{(P-N)}$ = 5.7 kJmol^{-1} for β-D-ddA, 20.2 kJmol^{-1} for β-D-ddG and 3.0 kJmol^{-1} for β-D-ddC; $\Delta\Delta H^{\circ}_{(D-N)}$ = -2.0 kJmol^{-1} for β-D-ddG and -1.9 kJmol^{-1} for β-D-ddT]. On the other hand, it can be also seen that the entropy of the system is efficiently modulated by the pD of the solution, both in the dN and ddN series.

(C) The strength of the anomeric effect and its modulation are weaker in β-D-dNs than β-D-ddNs counterparts.

Table 5. Pseudorotational analyses of temperature-dependent $^3J_{HH}$ (from 278 to 358 K)[a] at eleven different pDs (2.0-7.1), and determination of pD-dependent thermodynamics of the two state N ⇄ S equilibrium for α-D-dC (**20**).

	Total number of	Ψ_m constrained analyses in PSEUROT [b, c]		P_N and Ψ_m(N) constrained analyses in PSEUROT [c, d]		Slopes and intercepts of various van't Hoff plots from $\ln(x_S/x_N)$ vs 1000/T [f]		Thermodynamics of N ⇄ S equilibrium from van't Hoff plots [f, g]			Thermodynamics of N ⇄ S equilibrium from the average populations [h]
pD	PSEUROT analysis [e]	P_N	P_S	P_S	Ψ_m(S)	average slopes (σ)	average intercepts (σ)	ΔH° (σ)	-TΔS° (σ)	ΔG^{298} = ΔH°-TΔS°	ΔG^{298} = -0.298*R$\ln_{av}$ ($x_S/(x_N)$)
2.0	14926	-10° - 26°	157° - 173°	156° - 173°	30° - 36°	0.81 (0.07)	-0.97 (0.25)	-6.7 (0.6)	2.4 (0.6)	-4.3 (0.9)	-4.3 (0.2)
2.3	17312	-13° - 29°	157° - 175°	155° - 171°	30° - 36°	0.84 (0.11)	-1.11 (0.37)	-7.0 (0.9)	2.8 (0.9)	-4.3 (1.3)	-4.2 (0.2)
2.8	13871	-9° - 26°	155° - 169°	154° - 170°	30° - 36°	0.83 (0.07)	-1.06 (0.24)	-6.9 (0.6)	2.6 (0.6)	-4.3 (0.8)	-4.3 (0.2)
3.3	14382	-10° - 27°	155° - 171°	154° - 170°	30° - 36°	0.90 (0.07)	-1.31 (0.25)	-7.5 (0.6)	3.3 (0.6)	-4.2 (0.9)	-4.2 (0.2)
3.7	13061	-10° - 26°	155° - 178°	156° - 172°	29° - 36°	0.92 (0.07)	-1.46 (0.23)	-7.7 (0.6)	3.6 (0.6)	-4.1 (0.8)	-4.0 (0.2)
4.1	11255	-8° - 17°	157° - 171°	153° - 173°	30° - 36°	0.85 (0.06)	-1.37 (0.22)	-7.1 (0.5)	3.4 (0.5)	-3.7 (0.8)	-3.7 (0.2)
4.7	9679	-12° - 11°	157° - 171°	153° - 173°	29° - 34°	0.86 (0.06)	-1.56 (0.22)	-7.2 (0.5)	3.9 (0.5)	-3.3 (0.7)	-3.3 (0.2)
5.4	9738	-9° - 12°	159° - 177°	159° - 174°	29° - 34°	0.82 (0.06)	-1.46 (0.20)	-6.8 (0.5)	3.6 (0.5)	-3.2 (0.7)	-3.2 (0.2)
6.0	11105	-12° - 10°	161° - 181°	155° - 177°	29° - 34°	0.89 (0.06)	-1.73 (0.21)	-7.4 (0.5)	4.3 (0.5)	-3.2 (0.7)	-3.2 (0.2)
6.7	10326	-11° - 11°	158° - 174°	153° - 174°	28° - 34°	0.83 (0.06)	-1.53 (0.20)	-6.9 (0.5)	3.8 (0.5)	-3.1 (0.7)	-3.1 (0.2)
7.1	9262	-10° - 8°	157° - 172°	153° - 174°	28° - 34°	0.89 (0.06)	-1.71 (0.21)	-7.4 (0.5)	4.2 (0.5)	-3.2 (0.7)	-3.1 (0.2)

[a] $^3J_{HH}$ at each of eleven pDs at two extreme temperatures are given in Table 11. [b] Assuming Ψ_m (N) = Ψ_m (S), we have kept Ψ_m (N) and Ψ_m (S) fixed to identical values in the range from 29° to 37° at pD < 4.1, 28° to 36° at pD 4.1, 28° to 35° at pD > 4.1 and surveyed the hyperspace in 1° steps. [c] The error estimates of the PSEUROT analyses have been assessed in terms of ΔJ_{max} and r.m.s. The number of successful PSEUROT analyses in column 2 are designated to those which were within the constrained values (see experimental section) as well as having a ΔJ_{max} and r.m.s. values smaller than 0.6 Hz and 0.3 Hz, respectively. [d] P_N of the minor N-type conformers were fixed at -30° ≤ P_N ≤ 30° in 20° steps with Ψ_m (N) being simultaneously fixed at 29°, 33° and 37° at pD < 4.1, at 28°, 31° and 34° at pD ≥ 4.1 during several PSEUROT. [e] For each of these PSEUROT[22] calculations the coupling constants were 1000 times randomized which resulted in different populations of N and S conformers with their distinctive P_N and P_S (see experimental section). [f] The populations of N and S pseudorotamers obtained through each of the above PSEUROT calculations at different temperatures, shown in column 2, are the basis for the identical number of van't Hoff plots, which in turn were used to calculate the average slope and intercept. [g] The average of the slopes and the intercepts derived from all van't Hoff plots at a particular pD given in the columns 7 and 8 were finally used to calculate the average ΔH°, -TΔS° (at 298 K) and subsequently ΔG^{288} kJ/mol^{-1}) of N ⇄ S equilibria of **20**. [h] ΔG^{298} calculated directly from the average logarithm $\ln_{av}$ (x_S/ (1- x_S)), by using the Gibbs equation ΔG^T = -(RT/1000)$\ln_{av}$ (x_S/ (1- x_S)) with 1- x_S= x_N , R is the gas constant and T is the temperature. The standard deviations are in parentheses.

Assuming that the [O3'-C3'-C4'-O4'] and [O5'-C5'-C4'-O4'] gauche effects are constant factors in dNs, ddNs and abasic sugars 28 - 31, the different modulations of ΔH° of the pseudorotational equilibrium in dNs versus ddNs can be attributed to the different efficiency of the effect of the nucleobase. An estimate for the effect of the nucleobase [$\Delta H^{\circ}_{(AE)}$] in β-D-ddNs and β-D-dNs can be obtained through pairwise subtractions of their ΔH° values from the ΔH° value for the corresponding abasic sugar **28** (in the case of a ddN), **29** (in the case of a dN), **30** (in the case of 3'-OMe-β-D-dA) or **31** (in the case of 3',5'-OMe-β-D-dA).

In each of the protonated, neutral and deprotonated states of β-D-ddNs and β-D-dNs, the strength of the

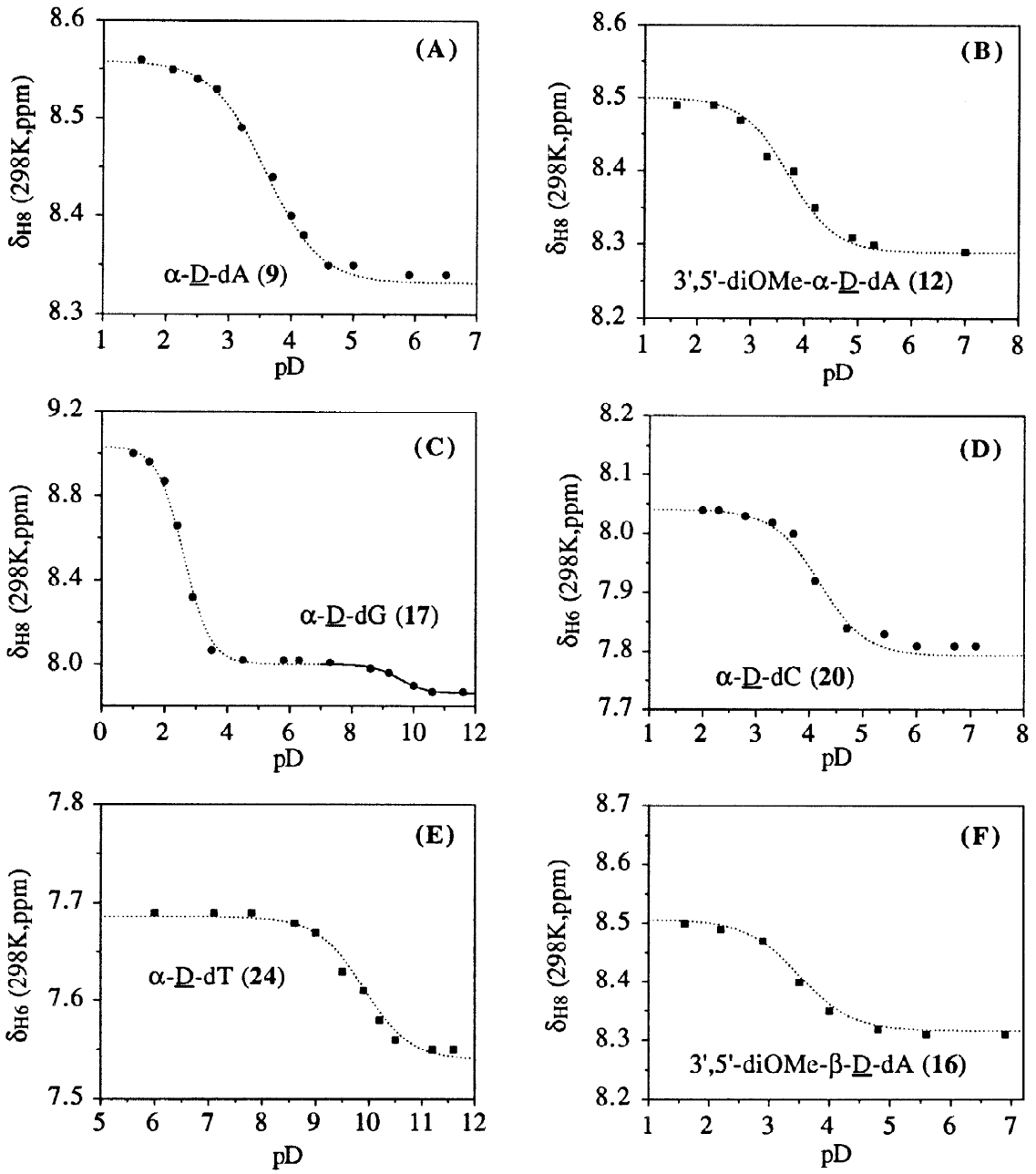

Fig 3 : pH-dependent chemical shift of the aromatic protons of the nucleobases in α-D-dNs (**9**), (**17**), (**20**) and (**24**), in 3',5'-diOMe-α-D-dA (**12**) and in 3',5'-diOMe-β-D-dA (**16**) (see ref. 2 for the β-D-dNs counterparts). **(A)** The sigmoidal dependence of the H8 chemical shift for α-D-dA (**9**) (at 12 pDs in the range 1.6 - 6.5) giving the pK_a of adenin-9-yl (3.6 ± 0.1). Similar plots (not shown) for H2 and H1' gave the same result. **(B)** The sigmoidal dependence of the H8 chemical shift for 3',5'-diOMe-α-D-dA (**12**) (at 9 pDs

in the range 1.5 - 7.0) giving the pK_a of adenin-9-yl (3.8 ± 0.1). A similar plot (not shown) for H1' gave the same result. **(C)** The sigmoidal dependence of the H8 chemical shift for α-D-dG (**17**) (at 14 pDs in the range 1.0 - 11.6) giving the pK_as of guanin-9-yl (2.6 ± 0.1 in the acidic pD range and 9.5 ± 0.1 in the alkaline pD range). A similar plot for H1' (not shown) in the acidic pD range gave the same result. **(D)** The sigmoidal dependence of the H6 chemical shift for α-D-dC (**20**) (at 11 pDs in the range 2.0 - 7.1) giving the pK_a of cytosin-1-yl (4.1 ± 0.1). A similar plot for H5 (not shown) gave the same result. **(E)** The sigmoidal dependence of the H6 chemical shift for α-D-T (**24**) (at 11 pDs in the range 6.0 - 11.6) giving the pKa of thymin-1-yl (9.9 ± 0.1). A similar plot for C5-Me protons (not shown) gave the same result. **(F)** The sigmoidal dependence of the H8 chemical shift for 3',5'-diOMe-β-D-dA (**16**) (at 8 pDs in the range 1.5 - 7.0) giving the pK_a of adenin-9-yl (3.5 ± 0.1). A similar plot (not shown) for H1' gave the same result.

anomeric effect, $\Delta H^{\circ}_{(AE)}$, can be calculated using Eqs 1 and 2, respectively:

$$\Delta H^{\circ}_{(AE)}\ (\beta\text{-D-ddN, P, N or D state}) = \Delta H^{\circ}\ (\beta\text{-D-ddA, } \beta\text{-D-ddG, } \beta\text{-D-ddC or } \beta\text{-D-ddT, Table 1}) - \Delta H^{\circ}\ (\textbf{28}\text{, Table 1}) \quad \text{..... Eq 1}$$

$$\Delta H^{\circ}_{(AE)}\ (\beta\text{-D-dN, P, N or D state}) = \Delta H^{\circ}\ (\beta\text{-D-dN, 3'-OMe-}\beta\text{-D-dN or 3',5'-diOMe-}\beta\text{-D-dN, Table 2}) - \Delta H^{\circ}\ (\textbf{29}\text{ in case of }\beta\text{-D-dN, }\textbf{30}\text{ in case of 3'-OMe-}\beta\text{-D-dN or }\textbf{31}\text{ in the case of 3',5'-diOMe-}\beta\text{-D-dN}) \quad \text{..... Eq 2}$$

The comparison of $\Delta H^{\circ}_{(AE)}$ (β-D-ddN) and $\Delta H^{\circ}_{(AE)}$ (β-D-dN) values in Table 8 leads us to the following conclusions: (i) The strength of the effect of the nucleobase is weakened by a factor of 2 - 4 in β-D-dNs in comparison with β-D-ddNs, which may be attributed to the reduced ability of O4' to be involved in $n(O4') \rightarrow \sigma^*_{C1'\text{-}N}$ orbital interactions with the σ* of C1'-N bond as it experiences the electron-withdrawing influence of 3'-OH moiety in dN series. (ii) The modulation of the strength of the effect of the nucleobase is considerably reduced in the dN series compared to the ddNs counterparts, which again shows the influence of the gauche effect of [O3'-C3'-C4'-O4'] in dNs.

(3) The nucleobase- and 3'-OH-dependent modulation of the sugar conformation in α-D-dNs operates either through tunable stereoelectronic forces and/or tunable entropy of the system

(A) The preferential anti orientation of the nucleobase around the glycosidic torsion in α-D-dNs prevents the interaction of 3'-OH proton with the nucleobase.

The estimates of the *syn / anti* ratios of conformers around the glycosidic torsion at one pD in each of the protonated, neutral and/or deprotonated states, for α-D-dNs **9**, **11**, **12**, **17**, **20** **24**, as obtained using Rosemeyer's method[27] basing on the results of 1D ^1H nOe difference experiments [see section (2)A] are collected in Table 7. The data in Table 7 reveal the followings.

(i) The predominance of *anti* rotamers for all α-D-dNs (except α-D-dG in alkaline solution) prevents the interaction of 3'-OH proton with N3 (in the case of purines) or O2 (in the case of pyrimidines) of the nucleobase. In β-D-dNs, as shown before, the nucleobase still predominantly adopts *anti*-type orientations, but this preference is reduced in comparison to the α-counterparts, and is further reduced at neutral pD compared to acidic pD.

(ii) The steric hindrance generated by 3'-OMe group in 3'-OMe-α-D-dA and 3',5'-diOMe-α-D-dA in comparison to 3'-OH in α-D-dA results in an increased preference of the nucleobase for *anti*-type rotamers

Table 6. Pseudorotational analyses of temperature-dependent $^3J_{HH}$ (from 278 to 358K)[a] at eleven pDs (6.0 - 11.6) and determination of the pD-dependent thermodynamics of the two-state N ⇄ S equilibrium in α-D-T (**24**).

	Total number of PSEUROT analyses [e]	Ψ_m constrained analyses in PSEUROT [b, c]		P_N and $\Psi_m(N)$ constrained analyses in PSEUROT [c, d]		Slopes and intercepts of various van't Hoff plots from $\ln(x_S/x_N)$ vs 1000/T [f]		Thermodynamics of N ⇄ S equilibrium from van't Hoff plots [f, g]			Thermodynamics of N ⇄ S equilibrium from the average populations [h]
pD		P_N	P_S	P_S	$\Psi_m(S)$	average slopes (σ)	average intercepts (σ)	ΔH° (σ)	-TΔS° (σ)	ΔG^{298} = ΔH°-TΔS°	ΔG^{298} = -0.298*R$\ln_{av}$ (x_S/x_N)
6.0	10362	-10° - 7°	154° - 187°	157° - 179°	26° - 33°	0.50 (0.05)	-0.84 (0.18)	-4.2 (0.4)	2.1 (0.5)	-2.1 (0.6)	-2.1 (0.2)
7.1	10832	-9° - 8°	152° - 189°	156° - 177°	26° - 32°	0.49 (0.05)	-0.78 (0.18)	-4.1 (0.4)	1.9 (0.5)	-2.1 (0.6)	-2.1 (0.2)
7.8	10449	-10° - 8°	152° - 186°	145° - 177°	26° - 32°	0.49 (0.05)	-0.81 (0.19)	-4.1 (0.4)	2.0 (0.5)	-2.1 (0.6)	-2.1 (0.2)
8.6	3982	-11° - 6°	152° - 185°			0.51 (0.05)	-0.87 (0.16)	-4.2 (0.4)	2.1 (0.4)	-2.1 (0.6)	-2.1 (0.2)
9.0	5526	-11° - 7°	155° - 192°			0.46 (0.05)	-0.77 (0.16)	-3.9 (0.4)	1.9 (0.4)	-1.9 (0.6)	-1.9 (0.1)
9.5	4489	-13° - 2°	150° - 188°			0.49 (0.05)	-0.95 (0.16)	-4.1 (0.4)	2.4 (0.4)	-1.7 (0.6)	-1.7 (0.1)
9.9	3269	-13° - 3°	151° - 192°			0.49 (0.05)	-1.01 (0.15)	-4.1 (0.4)	2.5 (0.4)	-1.6 (0.5)	-1.6 (0.1)
10.2	4381	-15° - 1°	149° - 190°			0.43 (0.05)	-0.91 (0.16)	-3.6 (0.4)	2.2 (0.4)	-1.3 (0.6)	-1.3 (0.1)
10.5	4210	-14° - 0°	150° - 192°			0.49 (0.05)	-1.14 (0.16)	-4.1 (0.4)	2.8 (0.4)	-1.2 (0.6)	-1.2 (0.1)
11.2	4597	-14° - 0°	149° - 192°			0.48 (0.05)	-1.13 (0.16)	-3.9 (0.4)	2.8 (0.4)	-1.2 (0.6)	-1.2 (0.1)
11.6	4431	-13° - 1°	151° - 194°			0.44 (0.05)	-1.04 (0.16)	-3.7 (0.4)	2.6 (0.4)	-1.1 (0.5)	-1.1 (0.1)

[a] $^3J_{HH}$ at each of the eleven pDs at two extreme temperatures are given in Table 12. [b] Assuming $\Psi_m(N) = \Psi_m(S)$, we have kept $\Psi_m(N)$ and $\Psi_m(S)$ fixed to identical values in the range from 27° to 33° at pD < 8.6, from 28° to 33° at pD 8.6, 26° to 33° at pD 9.0, 27° to 32° at pD 9.5, 28° to 33° at pD 9.9, 26° to 31° at pD 10.2, 10.5, 26° to 32° at pD 11.2 and 11.6 and surveyed the conformational hyperspace in 1° steps. [c] The error estimates of the PSEUROT analyses have been assessed in terms of ΔJ_{max} and r.m.s. The number of successful PSEUROT analyses in column 2 are designated to those which were within the constrained values (see experimental section) as well as having a ΔJ_{max} and r.m.s. values smaller than 0.6 Hz and 0.3 Hz. [d] P_N of the minor N-type conformers were fixed at -30° ≤ P_N ≤ 30° in 20° steps with Ψ_m (N) being simultaneously fixed at 17°, 30°and 33°at each pD < 8.6 during several PSEUROT optimizations. [e] For each of these PSEUROT[22] calculations the coupling constants were 1000 times randomized. [f] The populations of N and S pseudorotamers obtained through each of the above PSEUROT calculations at different temperatures, shown in column 2, are the basis for the identical number of van't Hoff plots, which in turn were used to calculate the average slopes and intercepts. [g] The average of the slopes and the intercepts derived from all van't Hoff plots at a particular pD given in the columns 7 and 8 were finally used to calculate the average ΔH°, -TΔS° (at 298 K) and subsequently ΔG^{298} (kJ/mol^{-1}) of N ⇄ S equilibria of **24**. [h] ΔG^{298} calculated directly from the average logarithm $\ln_{av}$ (x_S/ (1- x_S)), by using the Gibbs equation ΔG^T = -(RT/1000)$\ln_{av}$ (x_S/ (1- x_S)) with 1- x_S= x_N , R is the gas constant and T is the temperature. The standard deviations are in parentheses.

around the glycosidic torsion for 3'-OMe-α-D-dA and 3',5'-diOMe-α-D-dA compared to α-D-dA (see Table 7).

(iii) Noteworthy is the fact that in the case of ddNs[1], our results did not reveal any significant difference in the *syn/anti* ratios of rotamers around the glycosidic torsion for each of the α- versus β-D-ddN pairs, so that the relative intrinsic rigidity of the pentofuranose moiety in α- compared to β-D-ddNs could be specifically attributed to the inefficient transmission of the anomeric effect [n(O4')→$\sigma^*_{C1'\text{-}N}$ orbital overlap] in the former compared to the latter.

(B) The effect of 3'-OH on the flexibility of the sugar conformation in α-D-dNs is nucleobase-dependent

We have presented in the eqs 1 and 2 [Section (2)C] a procedure to estimate the strength of the effect of the nucleobase in β-D-ddNs [$\Delta H^\circ_{(AE)}$(β-ddN)] and β-D-dNs [$\Delta H^\circ_{(AE)}$(β-dN)]. Eqs 3 and 4, derived in a similar manner, enable the estimation of the strength of the effect of the nucleobase in α-D-ddNs and in α-D-dNs, respectively (see Table 8 for the results):

$\Delta H^\circ_{(AE)}$ (α-D-ddN in P, N or D state) = ΔH° (α-D-ddA, α-D-ddG, α-D-ddC or α-D-ddT, Table 1) - ΔH° (**28**, Table 1) ..... Eq 3

$\Delta H^\circ_{(AE)}$ (α-D-dN, P, N or D state) = ΔH° (α-D-dN, 3'-OMe-α-D-dN or 3',5'-diOMe-α-D-dN, Table 2) - ΔH° (**29** in case of α-D-dN, **30** in the case of 3'-OMe-α-D-dN or **31** in the case of 3',5'-diOMe-α-D-dN) ..... Eq 4

From the thermodynamic data presented in Table 1 for α-D-ddNs, Table 2 for α-D-dNs and Table 8 for the estimates of the effect of the nucleobase both in ddNs and dNs, following conclusions may be drawn.

(i) In the case of α-D-dA, its 3'-OMe and 3',5'-diOMe derivatives, both ΔH° and -TΔS° contributions to ΔG° of the pseudorotational equilibrium remain unchanged (in comparison with the neutral state) as adenin-9-yl becomes protonated [$\Delta\Delta H^\circ_{(P\text{-}N)}$ = 0.0 kJmol^{-1} and $\Delta(-T\Delta S^\circ)_{(P\text{-}N)}$ = 0.0 kJmol^{-1} for α-D-dA, $\Delta\Delta H^\circ_{(P\text{-}N)}$ = 0.6 kJmol^{-1} and $\Delta(-T\Delta S^\circ)_{(P\text{-}N)}$ = -1.1 kJmol^{-1} for 3'-OMe-α-D-dA and $\Delta\Delta H^\circ_{(P\text{-}N)}$ = 0.5 kJmol^{-1} and $\Delta(-T\Delta S^\circ)_{(P\text{-}N)}$ = -0.8 kJmol^{-1} for 3',5'-diOMe-α-D-dA]. This suggests that the strength of the stereoelectronic forces [*i.e.* the effect of the nucleobase and the gauche effect of (O3'-C3'-C4'-O4') fragment] that drive the sugar conformation in α-D-dA and its 3'-OMe and 3',5'-diOMe derivatives is pD-insensitive, as found earlier for α-D-ddA[1] (Table 8). The fact that -TΔS° of the pseudorotational equilibrium in α-D-dA is also pD-independent suggests that the relative proximity of the constituent 3'-OH and α-nucleobase does not, however, induce any steric hindrance.

(ii) On the other hand, as guanin-9-yl becomes protonated or deprotonated in α-D-dG, both ΔH° and -TΔS° contributions to ΔG° of the N⇄ S equilibrium change with respect to the neutral pD, as found previously for α-D-ddG[1]. The pD-dependent modulation of ΔH° of α-D-dG [$\Delta\Delta H^\circ_{(P\text{-}N)}$ = -6.2 kJmol^{-1} and $\Delta\Delta H^\circ_{(D\text{-}N)}$ = 1.1 kJmol^{-1}] is attributed to the resulting enhancement (upon protonation) or weakening (upon deprotonation) in the strength of the effect of the nucleobase (see Table 8). However, upon protonation of guanin-9-yl, it can be seen from Table 8 that the induced strengthening of the effect of the nucleobase is reduced by a factor of ≈ 1.5 in α-D-dG in comparison with α-D-ddG, showing the counteracting effect of 3'-OH in the former. The pD-dependent modulation of -TΔS° of the pseudorotational equilibrium in α-D-dG [$\Delta(-T\Delta S^\circ)_{(P\text{-}N)}$ = 3.7 kJmol^{-1} and $\Delta(-T\Delta S^\circ)_{(D\text{-}N)}$ = -1.3 kJmol^{-1}] as a result of the change of the electronic character

Table 7. The relative populations of *syn* versus *anti* rotamers around the glycosidic torsion in α-D-dNs **9**, **11**, **12**, **17**, **20** and **24** and in their β-D-counterparts **13**, **15**, **16**, **18**, **22** and **26** at various pDs [a] from 1D-nOe difference experiments[b].

Compound	pD	$\eta_{H1'}$ (%) (H6/H8 irradiated)	$\eta_{H6/H8}$ (%) (H1' irradiated)	$\frac{\eta_{H1'} + \eta_{H6/H8}}{2}$	% syn rotamers
α-D-dA (**9**) [c]	2.1	2.5	2.8	2.7	25
	6.5	5.4	4.0	4.7	44
3'-OMe-α-D-dA (**11**)	1.6	0.6	0.7	0.7	7
	6.9	1.2	0.9	1.1	10
3',5'-diOMe-α-D-dA (**12**)	1.6	1.0	0.9	1.0	10
	6.7	0.9	1.1	1.0	10
β-D-dA (**13**)	1.6	3.5	4.2	3.9	36
	6.9	5.8	5.9	5.9	55
3'-OMe-β-D-dA (**15**)	1.6	4.1	4.2	4.2	39
	7.0	5.5	6.5	6.0	56
3',5'-diOMe-β-D-dA (**16**)	2.2	2.4	2.4	2.4	22
	7.3	1.4	1.2	1.3	12
α-D-dG (**17**)	1.8	3.8	2.3	3.1	29
	7.3	4.7	2.3	3.5	33
	11.6	6.1	7.7	6.9	65
β-D-dG (**18**)	1.8	3.5	3.1	3.3	31
	7.7	3.8	4.0	3.9	36
	11.1	4.5	4.6	4.6	43
α-D-dC (**20**) [d]	2.0	0.9	-	0.9	8
	7.1	2.4	-	2.4	22
β-D-dC (**22**) [e]	7.3	2.8	2.8	2.8	26
α-D-T (**24**)	7.1	3.0	-	3.0	28
	11.6	3.4	-	3.4	32
β-D-T (**26**)	6.7	3.7	3.0	3.4	32
	11.7	3.1	2.4	2.8	26

[a] 1D-nOe difference experiments were performed in D_2O [298 K except for α-D-dG (**17**) and β-D-dG (**18**) (288 K) due to their decomposition above 288 K at acidic pDs]. [b] We used the method of Rosemeyer to calculate the population of *syn* rotamers around the glycosidic torsion from homonuclear ^1H nOes[27] (see the experimental section). [c] For α-D-dA (**9**), nOe difference experiments were performed at intermediate pDs (see the experimental section). [d] Selective saturation of H1' could not be performed at acidic pD for α-D-dC (**20**), due to the fact that H1' and H5 are near isochronous under these conditions. [e] Could not be measured in the acidic solution due to the fact that H1' and H5 in β-D-dC (**22**) have the same chemical shift at pD < 3 at 298 K.

Table 8. Estimation of the strength[a] of the effect of the nucleobase (AE, *i.e.* anomeric + steric) in α- or β-D-ddNs and in α- or β-D-dNs.

Compound	Effect of the Nucleobase (AE)[b]		
	'P' state	'N' state	'D' state
α-D-ddA (**1**)	-2.1	-2.1	-
β-D-ddA (**2**)	8.8	3.1	-
α-D-ddG (**3**)	-9.1	-0.8	-0.8
β-D-ddG (**4**)	23.2	3.0	1.0
α-D-ddC (**5**)	-3.3	-3.3	-
β-D-ddC (**6**)	9.2	6.2	-
α-D-ddT (**7**)	-	-1.5	-0.9
β-D-ddT (**8**)	-	5.0	3.1
α-D-dA (**9**)	-0.9	-0.9	-
3'-OMe-α-D-dA (**11**)	-1.2	-1.8	-
3',5'-diOMe-α-D-dA (**12**)	-0.9	-1.6	-
β-D-dA (**13**)	3.4	0.2	-
3'-OMe-β-D-dA (**15**)	3.2	0.0	-
3',5'-diOMe-β-D-dA (**16**)	3.2	0.6	-
α-D-dG (**17**)	-6.6	-0.4	0.7
β-D-dG (**18**)	6.2	1.3	-0.8
α-D-dC (**20**)	-3.0	-3.0	-
β-D-dC (**22**)	4.1	3.4	-
α-D-T (**24**)	-	0.1	0.1
β-D-T (**26**)	-	2.7	2.2

[a] In $kJmol^{-1}$. [b] The estimates of the effect of the aglycone have been calculated using Eq 1 for β-D-ddNs, Eq 2 for β-D-dNs, as well as for **15** and **16**, Eq 3 for α-D-ddNs and Eq 4 for α-D-dNs as well as for **11** and **12**.

of the constituent nucleobase cannot be unambiguously attributed to any steric hindrance generated by the spatial proximity of 3'-OH and the nucleobase.

(iii) The ΔH° of the N ⇄ S equilibrium in α-D-dC and α-D-T is not affected by pD [$\Delta\Delta H^\circ_{(P\text{-}N)}$ = 0.0 kJmol^{-1} for α-D-dC, $\Delta\Delta H^\circ_{(D\text{-}N)}$ = 0.0 kJmol^{-1} for α-D-T], whereas it is clearly pD-dependent for β-D-dC and β-D-T (as found earlier for α-D-ddC and α-D-ddT in comparison with β-D-ddC and β-D-ddT)[1]. This means that the effect of the nucleobase is not tuned by the change of pD in pyrimidine α-nucleosides, both in the dN and ddN series. However, the actual conformational preference (reflected in ΔG° value) of the sugar moiety in α-D-dC upon protonation or α-D-T upon deprotonation is clearly shifted toward N-type owing to the pD-dependent entropy change [$\Delta(-T\Delta S^\circ)_{(P\text{-}N)} = \Delta G^\circ_{(P\text{-}N)}$ = 1.5 kJmol^{-1} for α-D-dC; $\Delta(-T\Delta S^\circ)_{(D\text{-}N)} = \Delta G^\circ_{(D\text{-}N)}$ = 0.7 kJmol^{-1} for α-D-T]. This is in sharp contrast with α-D-ddC and α-D-ddT counterparts, where the sugar conformation remains the same at all pDs owing to the fact that -TΔS° term is also pD-independent. The pD-dependent flexibility of the sugar conformation of α-D-dC and α-D-T therefore shows the effect of pD-dependent steric interaction of the constituent 3'-OH and α-configured nucleobases.

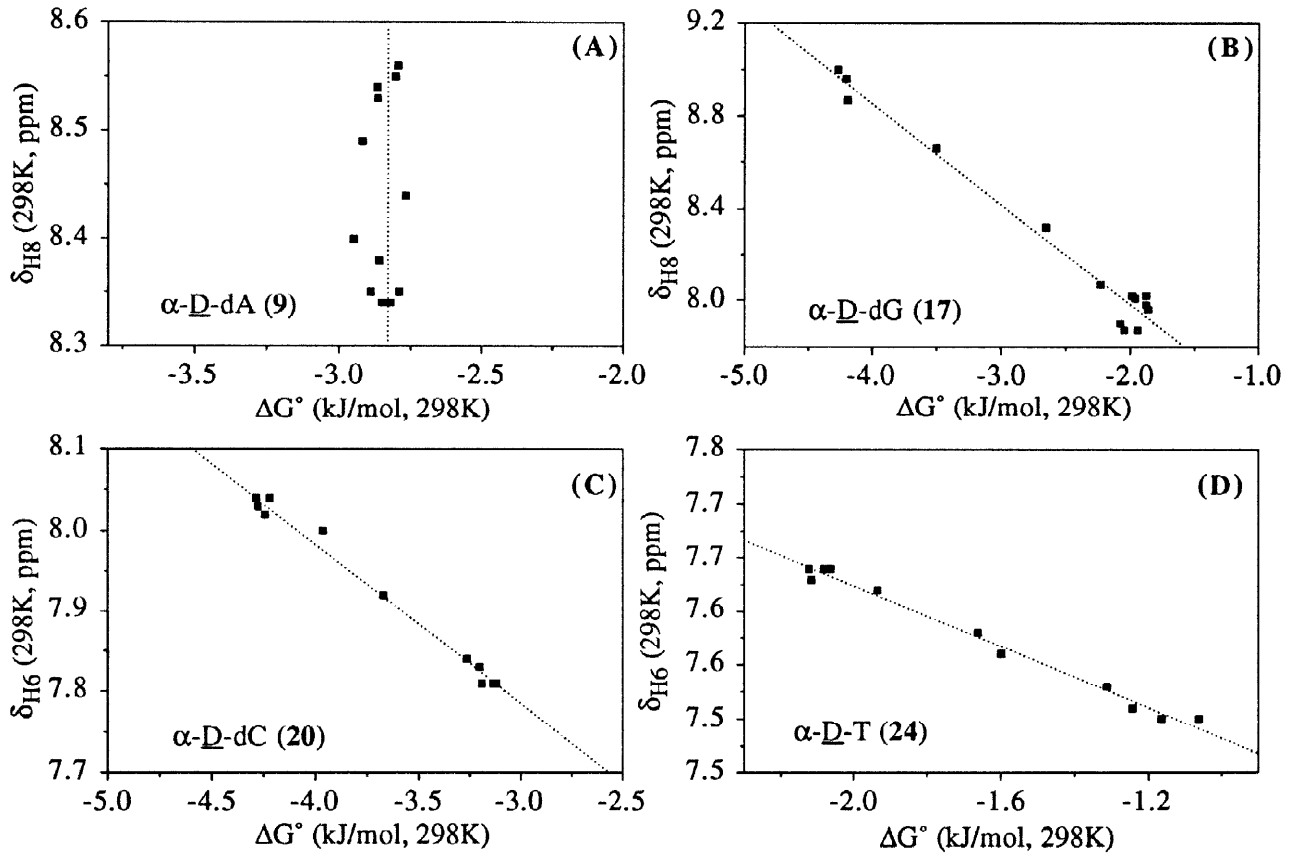

Fig 4 : The correlation plots of ^{1}H aromatic chemical shifts with ΔG° of the N⇄ S equilibrium in α-D-dNs **9, 17, 20** and **24. (A)** The plot of the pD-dependent H8 chemical shift (298 K) as a function of pD-dependent ΔG^{298} for the N⇄ S equilibrium of α-D-dA (**9**) giving a straight line that shows the inefficiency of the transmission of protonation/neutral equilibrium to drive the pseudorotational equilibrium (ΔG°). The intercept of the line with the ΔG° axis corresponds to the average ΔG° at any pD (see Table 2). **(B)** The correlation plot of the pD-dependent H8 chemical shift at 298 K as a function of pD-dependent ΔG^{298} for the N⇄ S equilibrium of α-D-dG (**17**) showing a straight line, with a correlation coefficient of 0.986, a slope of -0.43 (σ = 002) and an intercept of 7.11 (σ = 0.06). **(C)** The correlation plot of the pD-dependent H8 chemical shift (298 K) as a function of pD-dependent

ΔG^{298} for the N ⇄ S equilibrium of α-D-dC (**20**) showing a straight line with a correlation coefficient of 0.994, a slope of -0.20 (σ = 0.02) and an intercept of 7.18 (σ = 0.07). **(D)** The correlation plots of the pD-dependent H8 chemical shift (298 K) as a function of pD-dependent ΔG^{298} for the N ⇄ S equilibrium of α-D-T (**24**) showing a straight line with a correlation coefficient of 0.994, a slope of -0.14 (σ = 0.05) and an intercept of 7.39 (σ = 0.09).

(4) The comparison of the flexibility of the sugar conformation in α-D-dNs versus β-D-dNs.

(A) The ΔH° of the stereoelectronic forces in α-D-dNs are not efficiently modulated by the medium (i.e. pD) as compared to the β-D-counterparts

We have shown [Section (4)B] that the strength of the effect of the nucleobase is nearly pD-independent for α-D-dA, α-D-dC, α-D-T, whereas protonation and/or deprotonation of the nucleobase clearly shifts the bias of the N ⇄ S equilibrium toward N-type and S-type sugars, respectively, in their β-D-counterparts [see Section (2)B, C)]. This means that stereoelectronic forces (*i.e.* ΔH° term) are less efficiently transmitted to tune the sugar conformation in α-D-dNs than in β-D-dNs (except in the case of α-D-dG versus β-D-dG, where the extent of the pD-modulation is comparable). This is also consistent with what has already been observed in the case of α-D-ddNs with respect to their β-D-ddNs counterparts[1]: (i) The sugar moieties in α-D-ddA and α-D-ddC show the same conformational preferences at any pD. (ii) The deprotonation of guanin-9-yl in α-D-ddG and of thymin-1-yl in α-D-ddT does not yield any change of the conformation of the sugar moieties in comparison to neutral pD. (iii) On the other hand, ΔH° of the pseudorotational equilibrium is clearly affected by the pD of the medium for all β-D-ddN. This shows that the geometrical requirements necessary for the optimal orbital mixing [n(O4')→$\sigma^*_{C1'-N}$ orbital overlap] are intrinsically much reduced in α-D-dNs compared to β-D-dNs.

(B) The overall flexibility (ΔG°) of the sugar conformation in α-D-dNs is nucleobase-dependent because of the entropy penalty.

The data presented in Table 2 can be summarized as follows: (i) The change of the actual conformational preference (ΔG° term) of the sugar moiety in α-D-dC from the neutral to the protonated state and in α-D-T from the neutral to the deprotonated state is much greater than the corresponding modulation in β-D-dC and in β-D-T [$\Delta\Delta G^\circ_{(P\text{-}N)}$ = -1.2 kJmol^{-1} for α-D-dC, $\Delta\Delta G^\circ_{(D\text{-}N)}$ = 1.0 kJmol^{-1} for α-D-T, whereas $\Delta\Delta G^\circ_{(P\text{-}N)}$ = 0.5 kJmol^{-1} for β-D-dC, $\Delta\Delta G^\circ_{(D\text{-}N)}$ = -0.3 kJmol^{-1} for β-D-T]. (ii) The shift of the N⇄ S pseudorotational equilibrium from the neutral to the protonated state is comparable in α-D-dG and β-D-dG [$\Delta\Delta G^\circ_{(P\text{-}N)}$ = -2.5 kJmol^{-1} for α-D-dG and 1.6 kJmol^{-1} for β-D-dG]. (iii) However, from the perusal of the data in Table 1, it is also clear that the overall pD-dependent tunability of ΔG° upon the change of the pD of the medium is much larger in the β-D-ddNs than in the α-D-ddNs counterparts (compare the change in ΔG° values in the P, N, D states for each of the β-D-ddNs versus α-D-ddNs pairs). (v) The enhanced medium-dependent flexibility of the sugar conformation in α-D-dG, α-D-dC and α-D-T (the only exception is α-D-dA compared to β-D-dA) in comparison with their β-D-counterparts can therefore be attributed to the proximity of 3'-OH and the nucleobase in the α-face in the former, as evident in the overall pD-dependent entropy term.

(C) The comparison of the slopes of the correlation plots of δ^1H vs ΔG° of N⇄ S equilibrium further confirms that the pD-dependent entropy of the system in pyrimidine α-D-dNs results in the more efficient transmission of the energy (ΔG°) of the protonation/neutral/deprotonation equilibrium to drive the overall sugar conformation than in the β-D-series.

Fig 4 shows the plots of pD-dependent δ^1H of aromatic protons of the nucleobases in α-D-dNs **9, 17, 20** and **24** as a function of the free-energy (ΔG°) of their N ⇄ S equilibrium. All plots show straight lines with correlation coefficients above 0.99 except for α-D-dA, where ΔG° of the N ⇄ S equilibrium is pD-independent, which results in a straight line with infinite slope. The absolute values of the slopes of the straight lines shown in Fig 4 for α-D-dC and α-D-T (slope = -0.20 for α-D-dC, -0.14 for α-D-T) are smaller than for the corresponding β-D-dNs (see Fig 6 in ref. 2; slope = 0.53 for β-D-dC and 0.50 for β-D-T), showing that the pD-dependent entropy of the system is more efficient to drive the sugar conformation in the former compared to the latter. In purine nucleosides, the transmission of the protonation ⇄ deprotonation equilibrium to drive the sugar conformation, through the combined influence of stereoelectronic forces or the entropy of the system, is reduced in the α- compared to β-series, as shown by the larger slopes of the plots in Fig 4 for the former (slope = -0.43 for α-D-dG, slope infinite for α-D-dA) compared to the data published[2] for the latter (see Fig 6 in Ref. 2, slope = 0.28 for β-D-dA; 0.13 in the acidic pD-range and 0.69 in the alkaline pD-range for β-D-dG).

(5) The pK_as of the nucleobases are the same for each of the α- / β-D-dNs and the α- / β-D-ddNs pairs, showing that the electronic nature of the nucleobase is independent of the configuration at C1' and of the 3'-OH moiety.

Except for α-D-dA (**9**), the plots of the pD-dependent ΔG° (at 298K) of the N⇄ S equilibrium in α-D-dNs have the sigmoidal shape of titration curves, as originally found by us for β-D-dNs[2], which have been fitted to the Hasselbach-Henderson equation [Eq 5] to give the pK_as of the nucleobases at the inflection points (Fig 2) :

$$pD = pK_a + \log \frac{[A]}{[AH^+]} = pK_a + \log \frac{(1 - \alpha)}{\alpha} \quad \cdots\cdots \text{Eq 5}$$

α is calculated from the change in ΔG° values relative to the neutral state at a given pD divided by the total change in ΔG° value between the neutral and the protonated or the deprotonated state (Tables 3 - 6). These experimental pK_a values are completely consistent with those calculated from the pD-dependent chemical shifts of anomeric and aromatic protons in α-D-dNs according to the procedure described in our previous work[2] (Fig 3). The pK_as of the aglycones (Table 2) in α-D-dNs from pD-dependent free-energies of the N ⇄ S equilibrium and from pD-dependent chemical shifts of H8 or H6 protons (shown in parenthesis) are identical (within the NMR accuracy) to those of the β-counterparts[2,19]: 2.6 (2.6) for α-D-dG (**17**) and 2.3 (2.2) and 9.5 (9.5) for β-D-dG (**18**); 4.1 (4.1) for α-D-dC (**20**) and 4.2 (4.3) for β-D-dC (**22**); 9.7 (9.7) for α-D-T (**24**) and 9.7 (9.8) for β-D-T (**26**). The pK_a value of adenin-9-yl in α-D-dA (**9**) as well as the second pK_a for α-D-dG (**17**) could only be determined from pD-dependent chemical shift of H8 because of the fact that ΔG° of their pseudorotational equilibrium does not change from neutral to acidic pD in α-D-dA (**9**) and from neutral to alkaline pD in α-D-dG (**17**). The values found from pD-dependent chemical shifts are however identical for α-D-dA (**9**) (3.6) and its counterpart β-D-dA (**13**) (3.6), on one hand, for α-D-dG (**17**) (9.5) and β-D-dG (**18**) (9.5), on the other. All pK_a values reported here have been further verified by making Hill plots based both on the pD-dependent ΔG° values and ^{1}H chemical shifts. From the identical pK_a values we have obtained for α- and β-D-dNs, it can be concluded that any different conformational flexibilities that have been found above between α- and β-dNs is not the result of any different electronic nature of their constituent nucleobases, but owing to different orbital mixing of non-bonded O4' electron pair and the σ* of C1'-N bond[see section (4)]. Noteworthy is also the fact that the pK_a(s) of each nucleobase is (are) the same either in the β / α-D-dNs series

or in the β / α-D-ddNs counterparts, which clearly shows that 3'-OH moiety has no effect on the electronic nature of the nucleobase in dNs in comparison with ddNs.

(6) The mirror-image D- and L-dNs in either α- or β-forms are energetically equivalent within the timeframe and accuracy of NMR spectroscopy.

For each nucleobase, the pairwise comparison of the calculated ΔH° and ΔS° values of the N ⇄ S pseudorotational equilibria in α-D- and α-L-dNs, on one hand, and in β-D- and β-L-dNs, on the other, clearly shows that the D- and L-nucleosides within either α- or β-forms could not be energetically distinguished, as expected, because they exhibit identical pD-dependent conformational preferences (Tables 2 - 6). Note that the local minor differences observed between the ΔH° and ΔS° values for some of the D- versus L pairs result from the experimental inaccuracy of the pseudorotational analyses owing to the errors of the experimentally measured vicinal proton-proton coupling constants (See Tables 9 - 13 for $^3J_{HH}$ of α-D/L- and β-L-dNs and ref. 2 for $^3J_{HH}$ in β-D-dNs).

In fact, the above pairwise comparison of D and -L-nucleosides confirms the validity of the two-state N ⇄ S equilibrium as well as the accuracy of our procedure for the estimation of the thermodynamics[21] of the stereoelectronic forces that drive the sugar conformation.

Conclusion

This paper constitutes the first report delineating the inherent intramolecualr structural differences between the natural 2'-deoxynucleosides and their α counterparts. This paper also shows for the first time the interdependence of the aglycone promoted anomeric effect and the 3'-OH promoted gauche effect in 2'-deoxynucleosides compared to 2,3'-dideoxynucleosides that result into different conformational flexibilities as the medium changes. Our findings can be summarized as follows:

(1) For dNs, similarly to our previous results for ddNs[1], the aromatic characters of the nucleobases in α- and β-anomers are the same as evident from the identical pK_as of the constituent nucleobases in either α- or β-configuration.

(2) Owing to the predominant influence of the 3'-OH gauche effect over the anomeric effect, the sugar moiety adopts preferentially S-type conformations in β-D-dNs, whereas the anomeric effect alone drives the pseudorotational equilibrium toward N-type forms in the β-D-ddN counterparts. Owing to the cooperativity of the effect of the nucleobase and the gauche effect of [O3'-C3'-C4'-O4'] fragment, the population of S-type sugars in α-D-dNs is greater than in α-D-ddNs.

(3) The amplitude of the modulation of the strength of the anomeric effect by the pD of the solution is considerably reduced in all β-D-dNs compared to β-D-ddNs, and in α-D-dG compared to α-D-ddG, as a result of the gauche effect of 3'-OH in the dN series.

(4) The preferential *anti*-orientations of the nucleobases around the glycosidic torsion in all α-D-dNs as well as the almost identical conformational preferences in α-D-dA (**9**) and its derivatives, 3'-OMe-α-D-dA (**11**) and 3',5'-diOMe-α-D-dA (**12**), prompt us to conclude that there is no intramolecular interaction between 3'-OH proton and the nucleobase. As in α-D-ddA (**1**), the conformation of the sugar moiety in α-D-dA (**9**) is not pD-dependent, owing to the inefficiency of the transmission of stereoelectronic forces (*i.e.* anomeric effect) from the aglycone to steer the sugar conformation.

Table 9. The temperature-dependent vicinal coupling constants in α-D-dA (**9**) as a function of pD [a]

	α-D-dA (**9**)									
pD	$^3J_{1'2'}$		$^3J_{1'2''}$		$^3J_{2'3'}$		$^3J_{2''3'}$		$^3J_{3'4'}$	
	278 K	358 K	278 K	358 K	278 K	358 K	278 K	358 K	278 K	358 K
1.6[b]	7.4	7.4	2.3	2.7	6.4	6.7	2.5	2.8	2.6	3.0
2.1[b]	7.4	7.4	2.3	2.8	6.5	6.7	2.3	2.8	2.6	3.0
2.5[b]	7.4	7.5	2.3	2.8	6.5	6.6	2.3	3.0	2.6	3.3
2.8[b]	7.4	7.5	2.3	2.9	6.6	6.8	2.3	2.9	2.6	3.1
3.2[b]	7.5	7.5	2.4	3.0	6.6	7.0	2.4	2.8	2.6	3.1
3.7	7.6	7.6	2.5	3.1	6.7	7.1	2.3	2.9	2.7	3.1
4.0	7.7	7.6	2.5	3.1	6.7	7.0	2.4	2.9	2.6	3.2
4.2	7.7	7.6	2.5	3.2	6.6	7.1	2.4	2.9	2.6	3.2
4.6	7.7	7.7	2.5	3.2	6.8	7.1	2.3	2.9	2.6	3.2
5.0	7.7	7.7	2.5	3.1	6.7	7.1	2.4	3.0	2.5	3.1
5.9	7.7	7.7	2.6	3.1	6.7	7.1	2.5	3.0	2.6	3.1
6.5	7.7	7.7	2.6	3.2	6.8	7.1	2.4	3.0	2.6	3.2

[a] In Hz, error ± 0.1 Hz. Only $^3J_{HH}$ at the lowest and the highest temperature are tabulated. They are however available at several intermediate temperatures in 10 K steps. Note that complete set of $^3J_{HH}$ between 278 and 358 K at each pD have been used in the calculation of thermodynamic quantities through pseudorotational analyses and van't Hoff plots. Tabulated coupling constants are the result of simulation and iteration procedure by DAISY program.[29] [b] $^3J_{HH}$ for α-D-dA (**9**) could not be determined at pD = 1.6 above 328 K, at pD = 2.1 above 328 K, at pD 2.5, 2.8 and 3.2 above 348 K, because of its fast decomposition.

Table 10. The temperature-dependent vicinal coupling constants in α-D-dG (**17**) as a function of pD [a]

	α-D-dG (**17**)									
pD	$^3J_{1'2'}$		$^3J_{1'2''}$		$^3J_{2'3'}$		$^3J_{2''3'}$		$^3J_{3'4'}$	
	278 K	358 K	278 K	358 K	278 K	358 K	278 K	358 K	278 K	358 K
1.0[b]	7.1	7.1	1.4	1.7	5.9	5.9	1.7	2.1	1.7	2.2
1.5[b]	7.1	7.1	1.5	1.9	5.8	6.0	1.8	2.1	1.8	2.2
2.0[b]	7.1	7.2	1.6	1.9	5.9	6.2	1.9	2.2	1.8	2.2
2.4[b]	7.2	7.5	1.9	2.7	6.1	6.6	2.0	2.4	2.2	2.6
2.9[b]	7.4	7.6	2.4	3.1	6.5	7.1	2.2	2.7	2.6	3.2
3.5	7.7	7.7	2.9	3.6	6.9	7.1	2.5	3.4	2.9	3.5
4.5	7.7	7.6	3.0	3.5	7.1	7.1	2.4	3.3	2.9	3.5
5.8	7.7	7.7	3.0	3.5	6.7	7.2	2.9	3.2	2.9	3.5
6.3	7.8	7.7	3.0	3.5	6.9	7.1	2.6	3.4	3.1	3.4
7.3	7.7	7.7	3.0	3.5	6.9	7.1	2.7	3.4	3.0	3.4
8.6	7.8	7.7	3.0	3.5	6.9	7.1	2.7	3.3	2.8	3.2
9.2	7.9	7.8	3.0	3.5	6.8	7.0	2.7	3.2	2.9	3.5
10.0	8.1	8.0	3.1	3.4	7.0	7.3	2.5	3.0	2.7	3.0
10.6	8.2	8.0	3.1	3.5	6.8	7.2	2.5	2.9	2.8	3.2
11.6	8.2	8.0	3.1	3.5	6.8	7.2	2.4	2.7	2.9	3.2

[a] In Hz, error ± 0.1 Hz. Only $^3J_{HH}$ at the lowest and the highest temperature are tabulated, whereas they are available at several intermediate temperatures in 10 K or 5 K steps. Note that complete set of $^3J_{HH}$ between 278 and 358 K at each pD have been used in the calculation of thermodynamic quantities through pseudorotational analyses and van't Hoff plots. Tabulated coupling constants are the result of simulation and iteration procedure by DAISY program.[29] [b] $^3J_{HH}$ for α-D-dG (**17**) could not be determined at pD = 1.0 above 303 K, at pD = 1.5 and 2.0 above 308 K, at pD 2.4 above 328 K, at pD 2.9 above 338 K because of its fast decomposition.

Table 11. The temperature-dependent vicinal coupling constants in α-D-dC (**20**) as a function of pD [a,b]

	α-D-dC (**20**)									
pD	$^3J_{1'2'}$		$^3J_{1'2''}$		$^3J_{2'3'}$		$^3J_{2''3'}$		$^3J_{3'4'}$	
	278 K	358 K	278 K	358 K	278 K	358 K	278 K	358 K	278 K	358 K
2.0	6.9	7.0	1.8	2.5	5.8	5.9	1.9	2.5	1.6	2.4
2.3	6.9	7.0	1.8	2.4	5.7	5.9	1.9	2.4	1.6	2.2
2.8	6.9	7.0	1.8	2.7	5.8	6.0	1.9	2.5	1.7	2.5
3.3	6.9	7.1	1.8	2.7	5.8	6.0	1.9	2.6	1.7	2.6
3.7	7.0	7.2	1.9	2.8	6.0	6.0	1.9	2.7	1.6	2.6
4.1	6.9	7.2	2.0	3.0	5.9	6.3	2.1	2.9	1.8	2.7
4.7	7.0	7.2	2.3	3.3	6.0	6.4	2.1	2.9	1.8	2.9
5.4	7.0	7.2	2.3	3.3	5.9	6.4	2.3	3.0	2.0	3.0
6.0	7.1	7.2	2.3	3.4	6.0	6.5	2.3	3.3	1.9	2.8
6.7	7.0	7.2	2.3	3.4	6.0	6.5	2.4	3.2	2.0	2.9
7.1	7.0	7.2	2.3	3.4	6.0	6.5	2.1	3.1	2.1	2.9

[a] In Hz, error ± 0.1 Hz. Only $^3J_{HH}$ at the lowest and the highest temperature are tabulated, whereas they are available at several intermediate temperatures in 10 K steps. Note that complete set of $^3J_{HH}$ between 278 and 358 K at each pD have been used in the calculation of thermodynamic quantities through pseudorotational analyses. Tabulated coupling constants are the result of simulation and iteration procedure by DAISY program.[29] [b] $^3J_{HH}$ for α-D-dC (**20**) could not be determined at pD = 2.0, 2.8, 4.1, 5.4, 6.7 and 7.1 at 328 K, at pD = 2.3 above 338 K and at 328 K, at pD = 3.3 and 4.7 at 328 K and 338 K, at pD = 3.7 at 318 K and 328 K, at pD 6.0 at 308 K and 328 K due to the isochronicity of H3' and H4' resonances.

Table 12. The temperature-dependent vicinal coupling constants in α-D-T (**24**) as a function of pD [a]

	α-D-T (**24**)									
pD	$^3J_{1'2'}$		$^3J_{1'2''}$		$^3J_{2'3'}$		$^3J_{2''3'}$		$^3J_{3'4'}$	
	278 K	358 K	278 K	358 K	278 K	358 K	278 K	358 K	278 K	358 K
6.0	7.2	7.3	3.1	3.8	6.2	6.7	2.8	3.5	2.7	3.2
7.1	7.2	7.3	3.1	3.7	6.2	6.6	2.8	3.5	2.7	3.2
7.8	7.2	7.3	3.1	3.8	6.2	6.6	2.9	3.4	2.6	3.3
8.6	7.2	7.3	3.1	3.8	6.2	6.7	2.9	3.5	2.6	3.2
9.0	7.2	7.3	3.2	3.8	6.3	6.6	3.0	3.5	2.5	3.3
9.5	7.2	7.3	3.4	4.1	6.5	6.7	3.0	3.7	2.7	3.4
9.9	7.2	7.3	3.5	4.2	6.4	6.8	3.1	3.7	2.8	3.5
10.2	7.2	7.3	3.6	4.3	6.4	6.9	3.2	3.7	2.9	3.4
10.5	7.2	7.3	3.7	4.4	6.4	7.0	3.3	3.9	3.0	3.4
11.2	7.2	7.3	3.8	4.5	6.4	6.9	3.4	4.0	3.1	3.6
11.6	7.2	7.3	3.9	4.6	6.4	6.8	3.5	4.1	3.1	3.6

[a] In Hz, error ± 0.1 Hz. Only $^3J_{HH}$ at the lowest and the highest temperature are tabulated, whereas they are available at several intermediate temperatures in 10 K steps. The complete set of $^3J_{HH}$ between 278 and 358 K at each pD has been used to calculate the thermodynamic quantities through pseudorotational analyses and van't Hoff plots. Tabulated coupling constants are the result of simulation and iteration procedure by DAISY program.[29]

Table 13. The temperature-dependent vicinal coupling constants in α-L-dA (**10**), 3'-OMe-α-D-dA (**11**), 3',5'-diOMe-α-D-dA (**12**), β-L-dA (**14**), 3'-OMe-β-D-dA (**15**), 3',5'-diOMe-β-D-dA (**16**), β-L-dG (**19**), α-L-dC (**21**), β-L-dC (**23**), α-L-T (**25**) and β-L-T (**27**) as a function of pD [a]

Compound	pD	$^3J_{1'2'}$		$^3J_{1'2''}$		$^3J_{2'3'}$		$^3J_{2''3'}$		$^3J_{3'4'}$	
		278 K	358 K	278 K	358 K	278 K	358 K	278 K	358 K	278 K	358 K
α-L-dA (**10**)	1.8	7.4	7.4[b]	2.3	2.7[b]	6.5	6.7[b]	2.3	2.7[b]	2.7	3.1[b]
	6.4	7.7	7.7	2.5	3.2	6.7	7.0	2.2	2.9	2.6	3.2
3'-OMe-α-D-dA (**11**)	1.6	7.2	7.3[c]	1.5	1.8[c]	6.4	6.5[c]	1.5	1.7[c]	1.9	2.2[c]
	7.3	7.4	7.3	1.7	2.4	6.6	6.7	1.6	2.2	2.1	2.4
3',5'-diOMe-α-D-dA (**12**)	1.6	7.2	7.2[d]	1.7	2.0[d]	6.5	6.5[d]	1.6	2.0[d]	2.3	2.5[d]
	7.0	7.3	7.3	1.8	2.5	6.7	6.7	1.6	2.3	2.3	2.6
β-L-dA (**14**)	1.8	6.7	6.6[e]	6.5	6.6[e]	6.3	6.6[e]	4.1	4.2[e]	3.6	3.7[e]
	6.4	7.8	7.2	6.2	6.4	6.1	6.3	3.1	3.8	2.9	3.6
3'-OMe-β-D-dA (**15**)	1.6	7.4	7.3[f]	6.4	6.4[f]	6.1	6.3[f]	3.0	3.2[f]	2.8	3.0[f]
	7.3	8.5	7.8	6.0	6.2	5.8	6.2	2.3	2.9	2.3	2.8
3',5'-diOMe-β-D-dA (**16**)	1.6	7.0	6.9[g]	6.6	6.6[g]	6.2	6.3[g]	3.3	3.4[g]	3.2	3.3[g]
	6.9	7.6	6.9	6.3	6.5	6.2	6.4	3.0	3.5	2.8	3.5
β-L-dG (**19**)	1.2	5.7	5.7[h]	6.6	6.6[h]	6.4	6.5[h]	5.0	4.8[h]	4.1	4.0[h]
	7.0	7.6	7.1	6.3	6.5	6.2	6.5	3.4	3.9	3.1	3.6
	12.0	8.2	7.5	6.1	6.4	6.0	6.3	2.9	3.5	2.6	3.4
α-L-dC (**21**)	1.6	6.9	7.1	1.8	2.5	5.8	5.9	1.7	2.5	1.7	2.5
	7.3	7.1	7.2	2.4	3.4	6.0	6.5	2.1	3.2	2.1	2.9
β-L-dC (**23**)	1.8	6.3	6.4	6.5	6.6	6.6	6.6	4.4	4.4	3.9	4.1
	7.2	6.8	6.8	6.4	6.5	6.7	6.8	4.1	4.2	3.8	4.1
α-L-T (**25**)	7.2	7.2	7.3	3.1	3.8	6.1	6.6	2.8	3.5	2.7	3.2
	11.9	7.2	7.3	4.0	4.6	6.5	6.9	3.6	4.1	3.2	3.7
β-L-T (**27**)	6.6	7.0[i]	6.9	6.7[i]	6.7	6.7[i]	6.8	4.2[i]	4.3	4.1[i]	4.2
	11.9	7.4[j]	7.1	6.4[j]	6.6	6.9[j]	6.9	3.8[j]	4.1	4.1[j]	4.2

[a] In Hz, error ± 0.1 Hz. Only $^3J_{HH}$ at the lowest and the highest temperature are tabulated, whereas they are available at several intermediate temperatures in 10 K or 5 K steps. The set of $^3J_{HH}$ between 278 and 358 K at each pD have been used to calculate thermodynamic quantities through pseudorotational analyses and van't Hoff plots. Tabulated coupling constants result from simulation and iteration by DAISY program.[29] [b] At 323 K. $^3J_{HH}$ could not be extracted at this pD above 323 K due to the fast decomposition of α-L-dA (**10**). [c] At 328 K. $^3J_{HH}$ could not be extracted at this pD above 328 K due to the fast decomposition of 3'-OMe-α-D-dA (**11**). [d] At 328 K. $^3J_{HH}$ could not be extracted at this pD above 328 K due to the fast decomposition of 3',5'-diOMe-α-D-dA (**12**). [e] At 318 K. $^3J_{HH}$ could not be extracted at this pD above 318 K due to the fast decomposition of β-L-dA (**14**). [f] At 328 K. $^3J_{HH}$ could not be extracted at this pD above 328 K due to the fast decomposition of 3'-OMe-β-D-dA (**15**). [g] At 328 K. $^3J_{HH}$ could not be extracted at this pD above 328 K due to the fast decomposition of 3',5'-diOMe-β-D-dA (**16**). [h] At 308 K. $^3J_{HH}$ could not be extracted at this pD above 308 K due to the fast decomposition of β-L-dG (**19**). [i] At 328 K. $^3J_{HH}$ could not be extracted at this pD below 328 K due to the isochronicity of H2' and H2" resonances . [j] At 308 K. $^3J_{HH}$ could not be extracted at this pD below 308 K due to the isochronicity of H2' and H2" resonances.

(5) As in α-D-dA (**9**), the strength of the anomeric effect is not pD-modulated in α-D-dC (**20**) and α-D-T (**24**), which is consistent with our previous finding for α-D-ddC (**5**) and α-D-ddT (**7**). However, in α-D-dC (**20**) and α-D-T (**24**), the overall sugar conformation is considerably more altered than in β-D-dC and β-D-T, showing the effect of the steric proximity of 3'-OH and of the nucleobase in the α-face in pyrimidine α-D-dNs.

(6) We do not find any energetic basis of the chiral selection of the mirror-image D- or L-nucleosides since the free-energies of the stereoelectronic forces that dictate their respective inherent internal freedom in the aqueous solution are identical within the timeframe (~10^{-3} min) and the accuracy of measurement of the experimental energetics of the N ⇄ S equilibrium (±0.1-0.2 kJ/mol)[21]. The parity-violating energy difference[28] due to weak nuclear force, causing D-nucleosides to have a slightly favourable evolutionary bias because of slight energy stabilization over L-nucleosides, is so small (≈ 10^{-14} J mol^{-1} stabilization for D-ribose over L-ribose according to ab initio calculations[28e]) that it is not measurable by dynamic NMR spectroscopy.

Experimental Section

(I) ^{1}H-NMR spectroscopy.

(A) The temperature- and pD-dependent ^{1}H NMR at 500 MHz. ^{1}H-NMR spectra were recorded at 500 MHz (Bruker DRX 500) in D_2O solution [5 mM for α-D-dNs **9**, **17**, **20** and **24**, for **11**, **12**, **15** and **16**, α-L-dNs **10**, **21** and **25**, β-L-dNs **14**, **19**, **23** and **27** and for β-D-dG (**18**); 20 mM for β-D-dA (**13**), β-D-dC (**22**) and β-D-T (**26**), δ_{CH_3CN} = 2.00 ppm as internal reference] between 278 and 358 K at 5 K or 10 K intervals. For α-D-dNs **9**, **17**, **20** and **24**, the spectra have been recorded at various pDs in the following ranges: 1.6 - 6.5 for **9** (twelve pDs, see Table 9), 1.0 - 11.6 for **17** (fifteen pDs, see Table 10), 2.0 - 7.1 for **20** (eleven pDs, see Table 11), 6.0 - 11.6 for **24** (eleven pDs, see Table 12). In the case of L-nucleosides, **11**, **12**, **15**, **16**, ^{1}H-NMR spectra have been recorded only at two or three pDs at which their nucleobases are in the neutral, fully protonated or/and deprotonated forms, *i.e.* at pD 1.8 and 6.4 for α-L-dA (**10**), pD 1.6 and 7.3 for α-L-dC (**21**) and at pD 7.2 and 11.9 for α-L-T (**25**); at pD 1.8 and 6.4 for β-L-dA (**14**), pD 1.2, 7.0 and 12.0 for β-L-dG (**19**), pD 1.8 and 7.2 for β-L-dC (**22**) and at pD 6.6 and 11.9 for β-L-T (**27**) (see Table 13). The ^{1}H-NMR spectra have been recorded only at one pD (in the neutral range) for **28** - **31**. The pD ranges used to record the ^{1}H-NMR spectra of β-D-dNs **13**, **18**, **22** and **26** are reported in the Experimental Section in ref. 2. The pD values correspond to the reading on a pH meter equipped with a calomel electrode calibrated with two standard buffers in H_2O (pH 4 and 7) and are not corrected for the deuterium isotope effect. The pD of the samples has been adjusted by the simple addition of microliter volumes of concentrated D_2SO_4 or NaOD solutions. All spectra have been recorded using 64K data points and 16 or 32 scans. The assignments in **1** - **31** have been based on ^{1}H 1D homonuclear decoupling experiments. The relative assignments of H2' and H2", have been obtained from 1D ^{1}H-NOE difference experiments. In all dNs, H2' corresponds to the proton which lies on the same face of the pentofuranose moiety as H3', as a consequence of the mirror-image relationship of β-D-dNs with β-L-dNs, on one hand, of α-D-dNs with α-L-dNs, on the other (see Scheme 2). The pD-dependent accurate $^3J_{HH}$ (±0.1 Hz) have been obtained through simulation using DAISY program package[29] and have been used for the pseudorotational analyses [*vide infra*].

(B) The pD-dependent conformation about the glycosidic torsion from 1D nOe-diff experiments.

The NOEMULT pulse sequence included in the Bruker software package has been used to perform pD-

dependent 1D-NOE Diff experiments. The irradiation time of 3.2s with an irradiation power of 90 dB yielded a saturation ≤ 95%. The data were processed by sequential exponential multiplication (with 2 Hz or 4 Hz as the line broadening factor) and Fourier transformation of two FIDs (the first one corresponds to the irradiation of a specific multiplet, the second is OFF-resonance) and by subsequently subtracting both spectra.

1D-NOE Diff experiments have been preformed at various pD ranges for α-D-dNs (**9**, **17**, **20** and **24**), α-L-dNs (**10**, **21** and **25**) and β-D-dNs (**13**, **18**, **22** and **26**) to ascertain the position of their relative *syn* ⇄ *anti* equilibria[27]:

(a) For α-D-dA (**9**), irradiation of H8 yielded pD-dependent NOE enhancements at H1': 2.5% (at pD 2.1), 3.0% (at pD 2.5), 3.0% (at pD 2.8), 2.8% (at pD 3.5), 4.0% (at pD 4.0), 3.9% (at pD 4.6), 3.8% (at pD 5.9), 5.4% (at pD 6.5) whereas irradiation of H1' yielded pD-dependent NOE enahncements at H8: 2.8% (at pD 2.1), 3.4% (at pD 2.5), 3.2% (at pD 2.8), 3.8% (at pD 3.5), 4.6% (at pD 4.0), 3.6% (at pD 4.6), 4.5% (at pD 5.9), 4.0% (at pD 6.5). For α-D-dG (**17**), irradiation of H8 yielded pD-dependent NOE enhancements at H1' and H2", respectively: 3.7% and < 1.0% (at pD 1.3), 3.8% and < 1.0% (at pD 1.8), 3.0% and < 1.0% (at pD 2.0), 4.7% and 2.1% (at pD 7.3), 4.0% and 3.1% (at pD 8.6), 5.7% and 1.9% (at pD 10.6), 6.1% and 2.5% (at pD 11.6). For α-D-dC (**20**), irradiation of H6 resulted in NOE enhancements at H1' and H2", respectively: 0.9% and 0.7% (at pD 2.0), 2.2% and 1.3% (at pD 2.8), 2.3% and 1.6% (at pD 5.0), 2.4% and 1.3% (at pD 7.1). Finally, for α-D-T (**24**), irradiation of H6 yielded NOE enhancements at H1' and H2", respectively: 3.0% and 2.6% (at pD 7.1), 3.0% and 2.1% (at pD 8.6), 3.6% and 2.7% (at pD 10.2), 3.5% and 2.6% (at pD 10.5) and 3.4% and 2.5% (at pD 11.6).

(b) Irradiation of H8 in α-L-dA (**10**) resulted in NOE enhancements at H1' and H2", respectively: 1.8% and < 1% (at pD 1.6), 2.6% and 1.7% (at pD 7.6), whereas irradiation of H1' resulted in 1.5% (at pD 1.6), 3.0% (at pD 7.6) NOE enhancements at H8. Irradiation of H6 in α-L-dC (**21**) yielded < 1% (at pD 1.6) and < 1% (at pD 6.1) NOE enhancements at H2", whereas irradiation of H2" resulted in 1.7% (at pD 1.6) and 2.2% (at pD 6.1) NOE enhancements at H6. Irradiation of H6 in α-L-T (**25**) resulted in 2.3% and 2.2% (at pD 7.2), 2.6% and 2.4% (at pD 11.9) NOE enhancements at H1' and H2", respectively, whereas irradiation of H1' resulted in 2.2% (at pD 7.2) and 2.6% (at pD 11.9) NOE enhancement at H6.

(c) Irradiation of H8 in β-D-dA (**13**) resulted in NOE enhancements at H1', H3' and H2': 3.5%, 1.2% and 2.4% (at pD 2.0) and 4.3%, 0.9% and 2.5% (at pD 7.8), respectively, whereas irradiation of H1' yielded 3.9% (at pD 2.0) and 4.9% (at pD 7.8) NOE enhancements at H8. Irradiation of H8 in β-D-dG (**18**) resulted in NOE enhancements at H1', H3' and H2': 3.5%, 1.2% and 1.9% (at pD 1.8), 3.8%, 1.0% and 2.8% (at pD 3.8), 3.8%, 1.1% and 2.9% (at pD 7.7) and 4.5%, 0.6% and 2.2% (at pD 11.1), respectively, whereas irradiation of H1' resulted in 3.1% (at pD 1.8), 1.8% (at pD 3.8), 4.0% (at pD 7.7) and 4.6% (at pD 11.1) NOE enhancement at H8. Irradiation of H6 in β-D-dC (**22**) resulted in NOE enhancements at H3' and H2': 1.6% and 2.7% (at pD 1.8), 1.5% and 2.8% (at pD 4.2) and 1.4% and 2.9% (at pD 7.6), respectively, as well as 2.6% (at pD 4.2) and 2.7% (at pD 7.6) NOE enhancement at H1', whereas irradiation of H2' gives 5.8% (at pD 1.8), 6.0% (at pD 4.2) and 6.3% (at pD 7.6) NOE enhancement at H6. Finally, irradiation of H6 in β-D-T (**26**) resulted in NOE enhancements at H1' and H3', as follows: 2.9% and 2.2% (at pD 7.5), 3.1% and 2.0% (at pD 11.8), respectively, whereas irradiation of H1' resulted in 2.4% (at pD 7.5) and 2.2% (at pD 11.8) NOE enhancement at H6.

(II) The pD-dependent conformational preferences of the sugar moieties in 9 - 27 by pseudorotational analyses with PSEUROT program[22]

In dNs **9** - **27**, the five experimentally measured vicinal $^3J_{HH}$ have been used as input for the PSEUROT (version 5.4) program[22] to calculate the temperature-dependent bias of the two-state N⇄ S equilibrium at each pD in the ranges specified in the Experimental Section (I), (A). The iterated or simulated $^3J_{HH}$ have been interpretated in terms of two-state N⇄ S equilibrium[14] with the program PSEUROT[22], as they are time-average values of the $^3J_{HH}$ of the individual conformers. Five parameters are needed to describe the actual state of the N⇄ S equilibrium: The phase angles and puckering amplitudes of the N [P_N, $\Psi_m(N)$] and S [P_S, $\Psi_m(S)$] pseudorotamers and the mole fraction of one of them (x_N or x_S). PSEUROT calculates the best fit of these five parameters to the experimental $^3J_{HH}$. The input of a PSEUROT calculation consists of sets of (i) experimental $^3J_{HH}$, (ii) substituent electronegativities[22], and (iii) starting values for P_N, P_S, $\Psi_m(N)$ and $\Psi_m(S)$ as well as x_S at each temperature. PSEUROT is based on the pseudorotation concept[14] and on the new generalized Karplus equation[22b,c], which links $^3J_{HH}$ coupling constants to the corresponding proton-proton torsion angles on the basis of the "λ" substituent parameter scale[22d,e]. The following λ values have been used for the substituents attached to the H-C-C-H fragments : λ (C1') = λ (C3') = λ (C4') = 0.62, λ (C2') = 0.67, λ (C5') = 0.68, λ (O4') = 1.27, λ (OH) = 1.26 and λ (glycosyl-N) = 0.58[22d,e]. The proton-proton torsion angles in the pentofuranose moiety can be translated into the corresponding endocyclic torsion angles (ν_i, i = 0...4) by the PSEUROT program using relationships of the type: $\Phi_{HH} = B + A.\nu_i$. A and B parameters are as follows [in the case of α-D-dNs, we have subtracted 120° from the $\Phi_{1'2'}$ ($\Phi_{1'2''}$) values, whereas for α- and β-L-dNs A and B have been obtained by reversing the signs of both A and B values used for their α- and β-D counterparts, as suggested by Altona et al[20]]: A=1.06 and B=2.4 for $\Phi_{2'3'}$, A=1.06 and B=122.9 for $\Phi_{2''3'}$ and A=1.09 and B=-124.0 for $\Phi_{3'4'}$ in α-D-dNs and in β-D-dNs ; A=1.03 and B=121.4 for $\Phi_{1'2'}$, A=1.02 and B=0.9 for $\Phi_{1'2''}$ in β-DdNs and A=1.03 and B=1.4 for $\Phi_{1'2'}$, A=1.02 and B=-119.1 for $\Phi_{1'2''}$ in α-D-dNs; A=-1.06 and B=-2.4 for $\Phi_{2'3'}$, A=-1.06 and B=-122.9 for $\Phi_{2''3'}$ and A=-1.09 and B=124.0 for $\Phi_{3'4'}$ in α-L-dNs and in β-L-dNs; A=-1.03 and B=-121.4 for $\Phi_{1'2'}$, A=-1.02 and B=-0.9 for $\Phi_{1'2''}$ in β-L-dNs and A=-1.03 and B=-1.4 for $\Phi_{1'2'}$, A=-1.02 and B=119.1 for $\Phi_{1'2''}$ in α-L-dNs.

(a) Examination of the conformational hyperspace that is accessible to the N and S pseudorotamers. The PSEUROT analyses based on the experimentally measured $^3J_{HH}$ have been performed in two ways: (i) $\Psi_m(N)$ and $\Psi_m(S)$ were first assumed to be identical and constrained to the same value in a certain range (*vide infra*) during the PSEUROT calculation and (ii) when either the N or the S pseudorotamer is significantly preferred over the other (*i.e.* by ≥ 70%), P and Ψ_m of the minor conformer have been frozen to different sets of values (*vide infra*) while the geometry of the major pseudorotamer was optimized freely during the PSEUROT fitting process. The ensemble of PSEUROT analyses performed for each compound has been designed in order to carefully examine the hyperspace of geometries that are accessible to the N and S pseudorotamers and in such a way that the deviations between the experimental and back-calculated $^3J_{HH}$ (they are reflected in the value of ΔJ_{max}, *vide infra*) as well as the rms of the analyses remain minimal (*vide infra*). The detailed results of the PSEUROT analyses are given in the Tables 3 - 6 for α-D-dNs **9**, **17**, **20** and **24**.

(b) Investigation of the propagation of the error inherent to the experimental $^3J_{HH}$ in terms of the thermodynamics of the two-state N⇄ S equilibrium. For each set of starting geometries according to (a), we have generated typically 1000 - 3000 sets of $^3J_{HH}$ with a gaussian distribution (σ= 0.1 - 0.2 Hz) around the experimentally measured values. Each of these sets has been used as input for a PSEUROT calculation. The combination of (a) and (b) yielded typically 5000 - 20000 calculations for **9** - **27**.

(c) Van't Hoff type analysis of x_N and x_S calculated by PSEUROT to derive ΔH°, ΔS° of the N ⇄

S equilibrium. The temperature-dependent x_N and x_S calculated by PSEUROT have been subsequently used in 5000 - 20000 van't Hoff plots to obtain slopes and intercepts, which have been averaged to calculate the average enthalpy ($\Delta H°$) and entropy ($\Delta S°$) values of the N $\rightleftarrows$ S equilibrium in **9** - **27**. The free-energy (ΔG^T) of the N $\rightleftarrows$ S equilibrium at a certain temperature T can be calculated either by adding $\Delta H°$ and $-T\Delta S°$ or directly using the formula: $\Delta G^T = -RT*\ln_{av}(x_S / (1 - x_S))$ from the averaged logarithm of the ratio of x_S and x_N obtained at T with our PSEUROT analyses[1,22]. $\Delta G°$ values reported throughout this paper have been obtained using the second procedure.

(d) Results of the pseudorotational analyses for 3'-OMe-α-D-dA (11), 3',5'-diOMe-α-D-dA (12), 3'-OMe-β-D-dA (15), 3',5'-diOMe-β-D-dA (16), α-L-dNs (10, 21 and 25) and β-L-dNs (14, 19, 23 and 27). 3'-OMe-α-D-dA (**11**): $\Psi_m(N)$ and $\Psi_m(S)$ have been first constrained to the same value from 27° to 33° in 1° steps (at pD 1.6) and from 25° to 31° (at pD 7.3). P_N and P_S during these PSEUROTs are $-27° < P_N < 40°$ and $140° < P_S < 159°$ (at pD 1.6), $-35° < P_N < 19°$ and $142° < P_S < 160°$ (at pD 7.3). At each pD, P_N of the minor N pseudorotamer has been also constrained to $-30° < P_N < 30°$ in 20° steps with $\Psi_m(N)$ fixed at 27°, 30° and 33° (at pD 1.6) and at 25°, 28° and 31° (at pD 7.3), which resulted in $144° < P_S < 160°$ with $27° < \Psi_m(S) < 32°$ (at pD 1.6) and in $144° < P_S < 164°$ with $25° < \Psi_m(S) < 30°$ (at pD 7.3) ($\Delta J_{max} < 0.6$ Hz and rms < 0.3 Hz). The 19 sets of mole fractions of N- and S-type conformers at each pD were used to make the same number of van't Hoff plots. The average slopes and intercepts of these van't Hoff plots are respectively: 0.70 ($\sigma = 0.18$) and -0.32 ($\sigma = 0.59$) (at pD 1.6), 0.77 ($\sigma = 0.10$) and -0.77 ($\sigma = 0.30$) (at pD 7.3).

3',5'-diOMe-α-D-dA (**12**): $\Psi_m(N)$ and $\Psi_m(S)$ have been first constrained to the same value from 27° to 33° in 1° steps (at pD 1.6) and from 25° to 31° (at pD 7.0). P_N and P_S during these PSEUROTs are $-12° < P_N < 27°$ and $144° < P_S < 156°$ (at pD 1.6), $-27° < P_N < 18°$ and $139° < P_S < 156°$ (at pD 7.0). At each pD, P_N of the minor N pseudorotamer has been also constrained to $-30° < P_N < 30°$ in 20° steps with $\Psi_m(N)$ fixed at 27°, 30° and 33° (at pD 1.6) and at 25°, 28° and 31° (at pD 7.0), which resulted in $140° < P_S < 158°$ with $27° < \Psi_m(S) < 32°$ (at pD 1.6) and in $140° < P_S < 160°$ with $26° < \Psi_m(S) < 31°$ (at pD 7.0) ($\Delta J_{max} < 0.6$ Hz and rms < 0.3 Hz). The 19 sets of mole fractions of N- and S-type conformers at each pD were used to make the same number of van't Hoff plots. The average slopes and intercepts of these van't Hoff plots are respectively: 0.64 ($\sigma = 0.15$) and -0.31 ($\sigma = 0.49$) (at pD 1.6), 0.70 ($\sigma = 0.10$) and -0.66 ($\sigma = 0.27$) (at pD 7.0).

3'-OMe-β-D-dA (**15**): $\Psi_m(N)$ and $\Psi_m(S)$ have been first constrained to the same value from 29° to 35° in 1° steps (at pD 1.6) and from 30° to 36° (at pD 7.3). P_N and P_S during these PSEUROTs are $-29° < P_N < 24°$ and $145° < P_S < 176°$ (at pD 1.6), $-31° < P_N < 26°$ and $145° < P_S < 163°$ (at pD 7.3). At each pD, P_N of the minor N pseudorotamer has been also constrained to $-30° < P_N < 30°$ in 20° steps with $\Psi_m(N)$ fixed at 29°, 32° and 35° (at pD 1.6) and at 30°, 33° and 36° (at pD 7.3), which resulted in $145° < P_S < 173°$ with $29° < \Psi_m(S) < 36°$ (at pD 1.6) and in $145° < P_S < 165°$ with $31° < \Psi_m(S) < 37°$ (at pD 7.3) ($\Delta J_{max} < 0.6$ Hz and rms < 0.3 Hz). The 19 sets of mole fractions of N- and S-type conformers at each pD were used to make the same number of van't Hoff plots. The average slopes and intercepts of these van't Hoff plots are respectively: 0.17 ($\sigma = 0.07$) and 0.30 ($\sigma = 0.26$) (at pD 1.6), 0.55 ($\sigma = 0.05$) and -0.56 ($\sigma = 0.18$) (at pD 7.3).

3',5'-diOMe-β-D-dA (**16**): $\Psi_m(N)$ and $\Psi_m(S)$ have been first constrained to the same value from 29° to 35° in 1° steps (at pD 1.6) and from 30° to 36° (at pD 6.9). P_N and P_S during these PSEUROTs are $-9° < P_N < 33°$ and $149° < P_S < 182°$ (at pD 1.6), $-25° < P_N < 31°$ and $141° < P_S < 169°$ (at pD 6.9). At each pD, P_N of the minor N pseudorotamer has been also constrained to $-30° < P_N < 30°$ in 20° steps with $\Psi_m(N)$ fixed at 29°, 32° and 35° (at pD 1.6) and at 30°, 33° and 36° (at pD 6.9), which resulted in $142° < P_S < 182°$ with $28° < \Psi_m(S) <$

36° (at pD 1.6) and in 139° < P_S < 168° with 29° < Ψ_m(S) < 36° (at pD 6.9) (ΔJ_{max} < 0.6 Hz **and rms < 0.3** Hz). The 19 sets of mole fractions of N- and S-type conformers at each pD were used to make the same number of van't Hoff plots. The average slopes and intercepts of these van't Hoff plots are respectively: 0.12 (σ = 0.07) and 0.30 (σ = 0.24) (at pD 1.6), 0.43 (σ = 0.05) and -0.60 (σ = 0.17) (at pD 6.9).

α-L-dA (**10**): Ψ_m(N) and Ψ_m(S) have been first constrained to the same value from 24° to 33° in 1° steps at pD 1.8 and at pD 6.4. P_N and P_S during these 10 PSEUROTs are 2° < P_N < 32° and 145° < P_S < 162° (at pD 1.8), 0° < P_N < 38° and 149° < P_S < 194° (at pD 6.4). At each pD, P_N of the minor N pseudorotamer has been also constrained to -30° < P_N < 30° in 20° steps with Ψ_m(N) fixed at 24°, 28° and 32°, which resulted in 138° < P_S < 167° with 25° < Ψ_m(S) < 33° (at pD 1.8) and in 140° < P_S < 180° with 21° < Ψ_m(S) < 28° (at pD 6.4) (ΔJ_{max} < 0.6 Hz and rms < 0.3 Hz). The 22 sets of mole fractions of N- and S-type conformers at each pD were used to make the same number of van't Hoff plots. The average slopes and intercepts of these van't Hoff plots are respectively: 0.66 (σ = 0.11) and -1.09 (σ = 0.37) (at pD 1.8), 0.72 (σ = 0.06) and -1.27 (σ = 0.24) (at pD 6.4).

β-L-dA (**14**): Ψ_m(N) and Ψ_m(S) have been first constrained to the same value from 29° to 36° in 1° steps (at pD 1.8) and from 30° to 36° (at pD 6.4). P_N and P_S optimized during these 8 (at pD 1.8) or 7 (at pD 6.4) PSEUROTs are -20° < P_N < 25° and 140° < P_S < 171° (at pD 1.8) and -22° < P_N < 24° and 142° < P_S < 160° (at pD 6.4). At pD 6.4, P_N of the minor N pseudorotamer has been also constrained to -30° < P_N < 30° in 20° steps with Ψ_m(N) fixed at 30°, 33° and 36° which resulted in 140° < P_S < 166° with 31° < Ψ_m(S) < 38° (ΔJ_{max} < 0.6 Hz and rms < 0.3 Hz). The 8 sets (at pD 1.8), 19 sets (at pD 6.4) of mole fractions of N- and S-type conformers at each pD were used to make the same number of van't Hoff plots. The average slopes and intercepts of these van't Hoff plots are respectively: 0.14 (σ = 0.08) and -0.05 (σ = 0.26) (at pD 1.8), 0.47 (σ = 0.05) and -0.72 (σ = 0.15) (at pD 6.4).

β-L-dG (**19**): Ψ_m(N) and Ψ_m(S) have been first constrained to the same value from 29° to 36° in 1° steps (at pD 1.2), 30° to 36° (at pD 7.0) and from 31° to 37° (at pD 12.0). P_N and P_S optimized during these 8 (at pD 1.2) or 7 (at pD 7.0 and 12.0) PSEUROTs are -21° < P_N < 3° and 140° < P_S < 167° (at pD 1.2), -15° < P_N < 30° and 139° < P_S < 163° (at pD 7.0), and -17° < P_N < 34° and 146° < P_S < 164° (at pD 12.0). Additionally, at pD 7.0 and 12.0, P_N of the minor N pseudorotamer has been also constrained to -30° < P_N < 30° in 20° steps with Ψ_m(N) fixed at 30°, 33° and 36° (at pD 7.0) and at 31°, 34° and 37° (at pD 12.0) which resulted in 139° < P_S < 166° with 30° < Ψ_m(S) < 37° (at pD 7.0) and 142° < P_S < 164° with 31° < Ψ_m(S) < 38° (at pD 12.0) (ΔJ_{max} < 0.6 Hz and rms < 0.3 Hz). The 8 sets (at pD 1.2), 19 sets (at pD 7.0 and 12.0) of mole fractions of N- and S-type conformers at each pD were used to make the same number of van't Hoff plots. The average slopes and intercepts of these van't Hoff plots are respectively: -0.16 (σ = 0.09) and 0.63 (σ = 0.32) (at pD 1.2), 0.32 (σ = 0.04) and -0.36 (σ = 0.15) (at pD 7.0), 0.51 (σ = 0.05) and -0.68 (σ = 0.16) (at pD 12.0).

α-L-dC (**20**): Ψ_m(N) and Ψ_m(S) have been first constrained to the same value from 29° to 37° in 1° steps (at pD 1.6) and from 27° to 34° (at pD 7.3). P_N and P_S during these 9 (at pD 1.6) or 8 (at pD 7.3) PSEUROTs are -9° < P_N < 30° and 155° < P_S < 168° (at pD 1.6), and -11° < P_N < 9° and 157° < P_S < 187° (at pD 7.3). Additionally, at each pD, P_N of the minor N pseudorotamer has been also constrained to -30° < P_N < 30° in 20° steps with Ψ_m(N) fixed at 30°, 33° and 36° (at pD 1.6) and at 28°, 31° and 34° (at pD 7.3) which resulted in 154° < P_S < 171° with 30° < Ψ_m(S) < 36° (at pD 1.6) and in 152° < P_S < 175° with 28° < Ψ_m(S) < 34° (at pD 7.3) (ΔJ_{max} < 0.6 Hz and rms < 0.3 Hz). The 21 sets (at pD 1.6) and 17 sets (at pD 7.3) of mole fractions of N- and S-type conformers at each pD were used to make the same number of van't Hoff plots. The average slopes

and intercepts of these van't Hoff plots are respectively: 0.87 (σ = 0.07) and -1.21 (σ = 0.25) (at pD 1.6), 0.86 (σ = 0.06) and -1.65 (σ = 0.21) (at pD 7.3).

β-L-dC (**23**): $\Psi_m(N)$ and $\Psi_m(S)$ have been constrained to the same value from 29° to 36° in 1° steps (at pD 1.8) and from 29° to 37° (at pD 7.2). P_N and P_S optimized during these 8 (at pD 1.8) or 9 (at pD 7.2) PSEUROTs are -27° < P_N < 3° and 130° < P_S < 151° (at pD 1.8), and -24° < P_N < 10° and 129° < P_S < 1447 (at pD 7.2) (ΔJ_{max} < 0.6 Hz and rms < 0.3 Hz). The 8 sets (at pD 1.8) and 9 sets (at pD 7.2) of mole fractions of N- and S-type conformers at each pD were used to make the same number of van't Hoff plots. The average slopes and intercepts of these van't Hoff plots are respectively: 0.02 (σ = 0.04) and 0.23 (σ = 0.12) (at pD 1.8), 0.09 (σ = 0.04) and 0.21 (σ = 0.12) (at pD 7.2).

α-L-T (**25**): $\Psi_m(N)$ and $\Psi_m(S)$ have been first constrained to the same value from 25° to 33° in 1° steps (at pD 7.2) and from 24° to 32° (at pD 11.9). P_N and P_S optimized during these 9 PSEUROTs are -10° < P_N < 7° and 156° < P_S < 192° (at pD 7.2), and in -17° < P_N < 0° and 148° < P_S < 191° (at pD 11.9). Additionally, at pD 7.2, P_N of the minor N pseudorotamer has been also constrained to -30° < P_N < 30° in 20° steps with $\Psi_m(N)$ fixed at 26°, 29° and 32° which resulted in 151° < P_S < 179° with 26° < $\Psi_m(S)$ < 33° (ΔJ_{max} < 0.6 Hz and rms < 0.3 Hz). The 18 sets (at pD 7.2) and 9 sets (at pD 11.9) of mole fractions of N- and S-type conformers at each pD were used to make the same number of van't Hoff plots. The average slopes and intercepts of these van't Hoff plots are respectively: 0.51 (σ = 0.05) and -0.86 (σ = 0.18) (at pD 7.2), 0.41 (σ = 0.04) and -0.99 (σ = 0.16) (at pD 11.9).

β-L-T (**27**): $\Psi_m(N)$ and $\Psi_m(S)$ have been constrained to the same value from 29° to 36° in 1° steps (at pD 6.6) and from 30° to 36° (at pD 11.9). P_N and P_S optimized during these various PSEUROTs are -13° < P_N < 37° and 131° < P_S < 158° (at pD 6.6), and in -26° < P_N < 37° and 124° < P_S < 149° (at pD 11.9) (ΔJ_{max} < 0.6 Hz and rms < 0.3 Hz). The 8 sets (at pD 6.6) and 7 sets (at pD 11.9) of mole fractions of N- and S-type conformers at each pD were used to make the same number of van't Hoff plots. The average slopes and intercepts of these van't Hoff plots are respectively: 0.14 (σ = 0.14) and -0.02 (σ = 0.40) (at pD 6.6), 0.28 (σ = 0.08) and -0.25 (σ = 0.25) (at pD 11.9).

Acknowledgements

We thank the Swedish Technical Research Council (TFR), Swedish Natural Science Research (NFR) Council and Swedish Board for Technical Development (NUTEK) for generous financial support. Authors also thank Mr. J. Rong for initial preparation of some of the compounds used in the present work, Dr. J. Plavec and Mr. P. Forgo for preliminary NMR studies. Thanks are due to the Wallenbergstiftelsen, Forskningsrådsnämnden and University of Uppsala for funds for the purchase of a 500 and 600 MHz Bruker AMX and DRX NMR spectrometers.

References

1. Thibaudeau, C.; Földesi; A; Chattopadhyaya, J. *Tetrahedron* **1997**, *53*, 14043.
2. Thibaudeau, C.; Plavec, J.; Chattopadhyaya, J. *J. Org. Chem.* **1996**, *61*, 266.
3. (a) Urata, H.; Ogura, E.; Shinohara, K.; Ueda, Y.; Akagi, M. *J. Am. Chem. Soc.* **1991**, *113*, 8174. (b) Doi, M.; Inoue, M.; Tomoo, K.; Ishida, T.; Ueda, Y.; Akagi, M. ; Urata, H. *J. Am. Chem. Soc.* **1993**, *115*, 10432.
4. Jyoce, G.F.; Visser, G.M.; van Boeckel, C.A.A.; van Boom, J.H.; Orgel, L.E.; van Westrenen, J. *Nature* **1984**, *310*, 602.
5. Kaplan, N.O.; Ciotti, M.M.; Stolzenbach, F.E.; Bachur, N.R. *J. Am. Chem. Soc.* **1955**, *77*, 813.
6. (a) Suzuki, S.; Suzuki, K.; Imai, T.; Suzuki, N.; Okuda, S. *J. Biol. Chem.* **1965**, *240* , 554. (b) Suzuki, K.;

Nakano, H.; Suzuki, S. *J. Biol. Chem.* **1967**, *242*, 3319.
7. Dinglinger, F.; Renz, P. *Hoppe-Seyler's Z. physiol. Chem.* **1971**, *362*, 1157.
8. (a) LePage, G.A.; Junga, I.G. *Mol. Pharmacol.* **1967**, *2*, 37. (b) LePage, G.A. *Can. J. Biochem.* **1968**, *46*, 655. (c) Perry, A.; LePage, G.A. *Cancer Res.* **1969**, *29*, 617. (d) Nakai, Y.; LePage, G.A. *Cancer Res.* **1972**, *32*, 2445. (e) Tamaoki, T.; LePage, G.A. *Cancer Res.* **1975**, *35*, 1015.
9. Bobek, M.; Bloch, A. *J. Med. Chem.* **1975**, *18*, 784.
10. Falke, D.; Range, K.; Arendes, J.; Müller, W.E.G. *Biochim. Biophys. Acta* **1979**, *563*, 36.
11. Christensen, L.F.; Broom, A.D.; Robins, M.J.; Bloch, A. *J. Med. Chem.* **1972**, *15*, 735.
12. Séquin, U. *Experientia* **1973**, *29*, 1059.
13. (a) Morvan, F.; Rayner, B.; Imbach, J.-L.; Chang, D.-K.; Lown, J.W. *Nucleic Acids Res.* **1987**, *15*, 4241. (b) Morvan, F.; Rayner, B.; Imbach, J.-L.; Lee, M.; Hartley, J.A.; Chang, D.-K.; Lown, J.W. *Nucleic Acids Res.* **1987**, *15*, 7027.
14. (a) Kilpatrick, J.E.; Pitzer, K.S. ; Spitzer, R. *J. Am. Chem. Soc.* **1947**, *69*, 2483. (b) Altona, C.; Sundaralingam, M. *J. Am. Chem. Soc.* **1972**, *94*, 8205. (c) Altona, C.; Sundaralingam, M. *J. Am. Chem. Soc.* **1973**, *95*, 2333.
15. (a) de Leeuw, H.P.M; Haasnoot, C.A.G. ; Altona, C. *Isr. J. Chem.* **1980**, *20*, 108. (b) Altona, C.; Francke, R.; de Haan, R.; Ippel, J.H.; Daalmans, G.J.; Westra Hoekzema, A.J.A.; van Wijk, J. *Magn. Res.on Chem.* **1994**, *32*, 670.
16. (a) Feigon, J.; Wang, A. H. -J.; van der Marel, G. A.; van Boom, J. H.; Rich, A. *Nucleic Acids Res.* **1984**, *12*, 1243. (b) Tran-Dinh, S.; Taboury, J.; Neumann, J. -M.; Huynh-Dinh, T.; Genissel, B.; Laglois d'Estaintot, B.; Igolen, J. *Biochemistry* **1984**, *23*, 1362.
17. (a) Davis, P. W.; Hall, K.; Cruz, P.; Tinoco, I.; Neilson, T. *Nucleic Acids Res.* **1986**, *14*, 1279. (b) Davis, P. W.; Adamiak, R. W.; Tinoco, I. *Biopolymers* **1990**, *29*, 109.
18. (a) Agback, P.; Sandstrom, A.; Yamakage, S. -I.; Sund, C.; Glemarec, C.; Chattopadhyaya, J. *J. Biochem. Biophys. Methods* **1993**, *27*, 229. (b) Agback, P.; Glemarec, C.; Yin, L.; Sandstrom, A.; Plavec, J.; Sund, C.; Yamakage, S. -I.; Wiswanadham, G.; Rousse, B.; Puri, N.; Chattopadhyaya, J. *Tetrahedron Lett.* **1993**, *34*, 3929.
19. Izatt, R. M.; Christensen, J.J .; Rytting, J. H. *Chem. Rev.* **1971**, *71*, 439.
20. Hoffmann, R.A.; van Wijk, J.; Leeflang, B.R.; Kamerling, J.P.; Altona, C.; Vliegenthart, J.F.G. *J. Am. Chem. Soc.*, **1992**, *114*, 3710.
21. (a) Plavec, J.; Tong, W.; Chattopadhyaya, J. *J. Am. Chem. Soc.* **1993**, *115*, 9734. (b) Plavec, J.; Garg, N.; Chattopadhyaya, J. *J. Chem. Soc., Chem. Commun.* **1993**, 1011. (c) Plavec, J.; Koole, L. H.; Chattopadhyaya, J. *J. Biochem. Biophys. Meth.* **1992**, *25*, 253. (d) Koole. L. H.; Buck, H. M.; Nyilas, A.; Chattopadhyaya, J. *Can J. Chem.* **1987**, *65*, 2089. (e) Koole, L. H.; Buck, H. M.; Bazin, H.; Chattopadhyaya, J. *Tetrahedron* **1987**, *43*, 2289. (f) Koole, L. H.; Plavec, J.; Liu, H.; Vincent, B. R.; Dyson, M. R.; Coe, P. L.; Walker, R. T.; Hardy, G. W.; Rahim, S. G.; Chattopadhyaya J. *J. Am. Chem. Soc.* **1992**, *114*, 9934. (g) Plavec, J.; Thibaudeau, C.; Viswanadham, G.; Sund, C.; Chattopadhyaya, J. *J. Chem. Soc., Chem. Commun.* **1994**, 781. (h) Thibaudeau, C.; Plavec, J.; Watanabe, K. A.; Chattopadhyaya, J. *J. Chem. Soc., Chem. Commun.* **1994**, 537. (i) Thibaudeau, C.; Plavec, J.; Garg, N.; Papchikhin, A.; Chattopadhyaya, J. *J. Am. Chem. Soc.* **1994**, *116*, 4038. (j) Plavec, J.; Thibaudeau, C.; Chattopadhyaya, J. *J. Am. Chem. Soc.* **1994**, *116*, 6558. (k) Thibaudeau, C.; Plavec, J.; Chattopadhyaya, J. *J. Am. Chem. Soc.* **1994**, *116*, 8033. (l) Plavec, J.; Thibaudeau, C; Chattopadhyaya, J. *Tetrahedron* **1995**, *51*, 11775. (m) Plavec, J.; Thibaudeau,, C.; Chattopadhyaya, J. in *How do the Energetics of the Stereoelectronic Gauche and Anomeric Effects Modulate the Conformation of Nucleos(t)ides ?*, International Union of Pure and Applied Chemistry, **1996**, in press.
22. (a) De Leeuw, F. A. A. M. and Altona, C. *J. Comp. Chem.* **1983**, *4*, 428 and PSEUROT, QCPE program No 463. (b) Diez, E.; Fabian, J. S.; Guilleme, J.; Altona, C. and Donders, L.A. *Mol. Phys.* **1989**, *68*, 49. (c) Donders, L. A.; de Leeuw, F. A. A. M. and Altona, C. *Magn. Reson. Chem.* **1989**, *27*, 556. (d) Altona, C.; Ippel, J.H.; Hoekzema, A. J. A. W.; Erkelens, C.; Groesbeek, G.; Donders, L.A. *Magn. Reson. Chem.* **1989**, *27*, 564. (e) Van Wijk, J., unpublished result.
23. Edward, J.T. *Chem. Ind. (London)* **1955**, 1102.
24. For review articles on the anomeric effect, see: (a) Tvaroska, I.; Bleha, T. *Adv. Carbohydr. Chem.* **1989**, *47*, 45. (b) Juaristi, E.; Cuevas, G. *Tetrahedron* **1992**, *48*, 5019. (c) Petillo, P. A.; Lerner, L. A. in *The Anomeric Effect and Associated Stereoelectronic Effects*, Thatcher, G. R .J. Ed., ACS Symposium Series: Washington, DC, **1993**, pp. 156. (d) Box, V. G. S. *Heterocycles* **1990**, *31*, 1157.
25. (a) Lucken, E. A. C. *J. Chem. Soc.* **1959**, 2954. (b) Romers, C.; Altona, C; Buys, H. R.; Havinga, E. *Top. Stereochem.* **1969**, 4, 39. (c) Perrin, C. L.; Armstrong, K. B.; Fabian, M. A. *J. Am. Chem. Soc.* **1994**, *116*, 715. (d) Salzner, U. *J. Org. Chem.* **1995**, *60*, 986. (e) Cosse-Barbi, A.; Watson, D. G.; Dubois, J. E. *Tetrahedron Lett.* **1989**, *30*, 163.
26. (a) Olson, W.K.; Sussman, J. L. *J. Am. Chem. Soc.* **1982**, *104*, 270. (b) Olson, W.K. *J. Am. Chem. Soc.* **1982**, *104*, 278. (c) Phillips, L.; Wray, V. *J. Chem. Soc., Chem. Commun.* **1973**, 90. (d) Brunck, T.K.; Weinhold, F. *J. Am. Chem. Soc.* **1979**, *101*, 1700. (e) Murcko, M.A.; DiPaola, R.A. *J. Am. Chem. Soc.* **1992**, *114*, 10010. (f) Wiberg, K.B.; Murcko, M.A.; Laidig, K.E.; MacDougall, P.J. *J. Phys. Chem.* **1990**, *94*, 6956.
27. Rosemeyer, H.; Tóth, G.; Golankiewicz, B.; Kazimierczuk, Z.; Bourgeois, W.; Kretschmer, U.; Muth, H.-P. and Seela, F. *J. Org. Chem.* **1990**, *55*, 5784.
28. (a) Lee, T.D.; Yang, C.N. *Phys. Rev.* **1956**, *104*, 254. (b) Quack, M. *Angew. Chem. Int. Ed. Engl.* **1989**, 28, 571. (c) Mason, S.F. *Chirality*, **1991**, *3*, 223. (d) Tranter, G.E. *Nature*, **1985**, 318, 172. (e) Tranter, G.E. *Chem. Phys. Lett.* **1987**, 135, 279. (f) Kondepudi, D.K.; Nelson, G.W.; *Nature*, **1985**, 314, 438.
29. DAISY, Spin Simulation Program, provided by Bruker, was used with 7 spins systems.